J. metamorphic Geol., 2012, **30,** 703–722 doi:10.1111/j.1525-1314.2012.00991.x

Role of chemical processes on shear zone formation: an example from the Grimsel metagranodiorite (Aar massif, Central Alps)

P. GONCALVES,[1] E. OLIOT,[1,2] D. MARQUER[1] AND J. A. D. CONNOLLY[3]
[1]*UMR-CNRS 6249 Chrono-Environnement, Université de Franche-Comté, 16 route de Gray 25030 Besançon cedex, France (philippe.goncalves@univ-fcomte.fr)*
[2]*UMR-CNRS 7516 Institut de Physique du Globe de Strasbourg, 1 rue Blessig, 67084 Strasbourg Cedex, France*
[3]*Earth Science Department, Swiss Federal Institute of technology, CH-8092 Zürich, Switzerland*

ABSTRACT Alpine deformation in the Grimsel granodiorite (Aar massif, Central Alps) at greenschist facies conditions (6.5 ± 1 kbar for 450°C ± 25°C) is characterized by the development of a network of centimetre to decametre localized shear zones that surround lenses of undeformed granodiorite. Localization of deformation is assumed to be the result of a first stage of extreme localization on brittle precursors (nucleation stage) followed by a transition to ductile deformation and lateral propagation into the weakly deformed granodiorite (widening stage). A paradox of this model is that the development of the ductile shear zone is accompanied by the crystallization of large amounts of phyllosilicates (white mica and chlorite) that maintains a weak rheology in the localized shear zone relative to the host rock so that deformation is localized and prevents shear zone widening. We suggest that chemical processes, and more particularly, the metamorphic reactions and metasomatism occurring during re-equilibration of the metastable magmatic assemblage induced shear zone widening at these *P–T–X* conditions. These processes (reactions and mass transfer) were driven by the chemical potential gradients that developed between the thermodynamically metastable magmatic assemblage at the edge of the shear zone and the stable white mica and chlorite rich ultramylonite formed during the first stage of shear zone due to localized fluid infiltration metasomatism. *P–T* and chemical potential projections and sections show that the process of equilibration of the wall rocks (μ–μ path) occurs via the reactions: kf + cz + ab + bio + MgO + H_2O = mu + q + CaO + Na_2O and cz + ab + bio + MgO + H_2O = chl + mu + q + CaO + Na_2O. Computed phase diagram and mass balance calculations predict that these reactions induce relative losses of CaO and Na_2O of ~100% and ~40% respectively, coupled with hydration and a gain of ~140% for MgO. Intermediate rocks within the strain gradient (ultramylonite, mylonite and orthogneiss) reflect various degrees of re-equilibration and metasomatism. The softening reaction involved may have reduced the strength at the edge of the shear zone and therefore promoted shear zone widening. Chemical potential phase diagram sections also indicate that the re-equilibration process has a strong influence on equilibrium mineral compositions. For instance, the decrease in Si-content of phengite from 3.29 to 3.14 p.f.u, when white mica is in equilibrium with the chlorite-bearing assemblage, may be misinterpreted as the result of decompression during shear zone development while it is due only to syn-deformation metasomatism at the peak metamorphic condition. The results of this study suggest that it is critical to consider chemical processes in the formation of shear zones particularly when deformation affects metastable assemblages and mass transfer are involved.

Key words: Aar massif; Central Alps; chemical potential phase diagram; metasomatism; shear zone.

INTRODUCTION

The formation of shear zones in a homogeneous plutonic host rock may be subdivided into two distinct stages: nucleation and development (e.g. Mancktelow & Pennacchioni, 2005). Although the early evidence of the nucleation stage is usually overprinted with the accumulation of deformation, it has been shown that shear zones may nucleate on pre-existing brittle structures (joints, veins and faults) either at the macroscopic or microscopic scale (Simpson, 1985; Segall & Simpson, 1986; Guermani & Pennacchioni, 1998; Montési & Zuber, 2002; Mancktelow & Pennacchioni, 2005; Pennacchioni, 2005; Pennacchioni & Mancktelow, 2007). The second stage corresponds to development of the ductile shear zone, which requires the maintenance of a weak rheology in a narrow domain relative to the host rock, so that deformation is localized rather than homogeneously spread throughout the rock (Rutter, 1999; Burlini & Bruhn, 2005; Holyoke & Tullis, 2006). This weakness is likely due to textural changes, such as grain-size reduction and formation of fined-grained polyphased aggregates that can deform by grain boundary sliding, development of a grain preferred orientation and/or interconnection of an initially dispersed weak phase, like mica (Poirier, 1980;

© 2012 Blackwell Publishing Ltd

Stunitz & Tullis, 2001; Oliot *et al.*, 2010). Fluid influx will also have a favourable softening effect by promoting a switch from dislocation creep to fluid-assisted grain-boundary diffusion creep and grain-boundary sliding (e.g. Tullis *et al.*, 1996). The maintenance of the weak rheology can also be promoted by dramatic mineral transformations due to syn-kinematic metamorphic reactions governed by changes in *P–T* conditions and fluid-rock interactions (Mitra, 1978; White & Knipe, 1978; McCaig, 1984; Gapais, 1989; Wintsch *et al.*, 1995, 2005; Wibberley, 1999; Yonkee *et al.*, 2003; Barnes *et al.*, 2004; Sassier *et al.*, 2006). These softening reactions can either produce weak phyllosilicates at the expense of framework silicates, like the feldspar to muscovite reaction (e.g. Gueydan *et al.*, 2003) or fine-grained assemblages, like albite-oligoclase aggregates, developed at the expense of magmatic plagioclase porphyroclasts under upper greenschist to amphibolite facies conditions (Oliot *et al.*, 2010).

In a single crystalline massif, shear zones with widths varying from millimetres to decametres are commonly described (Choukroune & Gapais, 1983; Fourcade *et al.*, 1989; Guermani & Pennacchioni, 1998). This variety in width of shear zones cannot be explained only by the maintenance of a weak rheology because the interplay of mechanical and chemical processes cited above should favour the accumulation of more strain in the narrow high strain zones and therefore prevent the lateral widening of the shear zones. Although some conceptual models involve a stage of shear zone widening (e.g. Ingles *et al.*, 1999), little is known about the processes involved. Two opposing models for shear zone broadening are proposed: (i) shear zone hardening and (ii) softening of the adjacent host-rock.

1. Hardening is the most popular model used to explain the thickening of the shear zone via the migration of the initially localized shear zone into adjacent host rock (Means, 1995; Vitale & Mazzoli, 2008). Increase in strength in the centre of the shear zone can be due to reaction-hardening, by the growth of porphyroblastic minerals like garnet or andalusite (Groome *et al.*, 2006), or due to strain-hardening, during the development of a deformation fabric or the change in deformation mechanism (as from dissolution–precipitation mechanisms to dislocation creep) (Johnson *et al.*, 2011).
2. Shear zone widening is expected if the strength of the adjacent host-rock decreases during deformation. Gueydan *et al.* (2003) suggested that shear zone widening in homogeneous granitoids is induced by the progressive transformation of strong K-feldspar of the host rock into white mica. These softening reactions affecting the adjacent host-rock are initiated by microfracturing of the coarse 'strong' grains and promoted by progressive fluid infiltration through these fractures (Ingles *et al.*, 1999; Gueydan *et al.*, 2003).

The chemical transformations, involved in all the stages of formation of a shear zone, are associated with transport of dissolved species either by diffusion through stationary pore fluids (diffusion metasomatism) or with fluids percolating through the pores of the rock (infiltration metasomatism) (Korzhinskii, 1970). Metasomatism has been reported and quantified in many shear zones when mass transfer occurred on a large scale (commonly greater than decimetre scale) (Marquer *et al.*, 1985; Marquer & Burkhard, 1992; Fitz Gerald & Stünitz, 1993; Wibberley, 1999; Yonkee *et al.*, 2003). Metasomatic reactions can significantly alter the bulk rock composition and produce mineral assemblages significantly different from those expected under closed-system conditions. Therefore, modelling the effects of mass transfer on phase relations (i.e. open system modelling) is critical to better understand how they can influence the formation of shear zones.

The fundamental question addressed in this contribution is: how a shear zone can widen a pre-existing fracture or a weak localized shear zone? We will emphasize the role of chemical processes (metamorphic reactions and mass transfer) on the widening stage and more particularly the major role of re-equilibration of metastable magmatic assemblages at the *P–T–X* conditions of deformation.

In this contribution, a synthesis is presented of the mineralogical and chemical changes observed along a strain gradient, located in the Grimsel granodiorite (Aar massif, Central Alps), from the undeformed and unaltered protolith to the most deformed rock (chlorite-bearing ultramylonite). After determining the *P–T* conditions of shear zone nucleation and widening, μ–μ phase diagram projections and sections are used to determine the reaction path of equilibration, to quantify the amount of mass transfer, and to assess the mineralogical evolution (composition and modes) during shear zone widening. Particular attention is paid to white mica, because of its critical impact on shear zone rheology and also because of its thermobarometric applications. We conclude with a conceptual model of shear zone formation where fluid-rock interactions and the resulting equilibration of the metastable magmatic assemblage is the main driving force of shear zone widening.

GEOLOGICAL SETTING AND SELECTED SAMPLES

The Aar massif belongs to the External Crystalline Massifs of the Central Alps, which have been thrust towards the northwest under greenschist facies metamorphic conditions during late Alpine tectonics (Steck, 1968, 1984; Choukroune & Gapais, 1983; Marquer *et al.*, 1985; Marquer, 1987). The Aar massif consists of pre-Variscan gneisses, and Palaeozoic migmatites and amphibolites that were intruded by numerous granitoids during the late Variscan orogeny (Labhart, 1977; Abrecht, 1994; Schaltegger, 1994). The Grimsel granodiorite and Aar granite are one of these Variscan intrusions exposed in the southern and central part of

© 2012 Blackwell Publishing Ltd

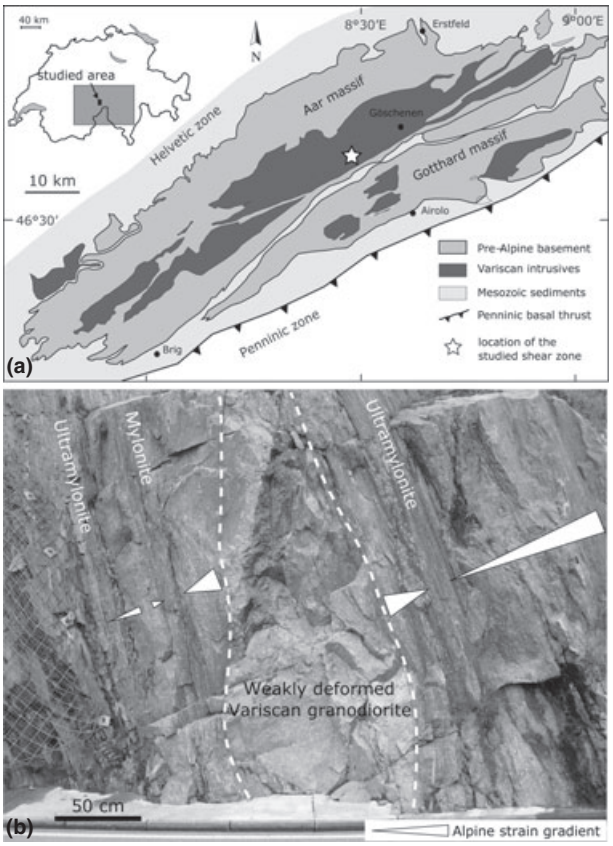

Fig. 1. (a) Simplified geological map of the External Crystalline Massifs (Aar and Gotthard) of the Central Alps (Switzerland) showing the location and extent of Variscan intrusives in the basement. (b) Outcrop showing the typical alpine heterogeneous deformation in the Grimsel granodiorite. Shear zones wrap around lens–shaped domains of weakly deformed granodiorite at different scales.

the Aar massif, a few kilometres north of the Grimsel pass (Fig. 1a).

Alpine deformation in the Grimsel granodiorite is heterogeneous and characterized by a network of anastomosing shear zones wrapping around lens-shaped domains of weakly deformed rocks at different scales (Choukroune & Gapais, 1983; Marquer *et al.*, 1985; Gapais *et al.*, 1987) (Fig. 1b). The metamorphic conditions of the Alpine ductile deformation in the Grimsel granodiorite have been estimated at 450 ± 30 °C and 6 ± 1 kbar, according to $\delta^{18}O$ analyses of biotite and quartz (Fourcade *et al.*, 1989) and the Si-content in phengite (3.2 & 3.3 p.f.u.) from various shear zones (Challandes *et al.*, 2008). The ductile deformation has been dated at 21–17 Ma by ^{39}Ar–^{40}Ar on recrystallized biotite and phengite from two shear zones (Challandes *et al.*, 2008).

The modelling of metasomatic phase relations in this paper is applied to a well-characterized decametre-sized Alpine shear zone developed in the Variscan Grimsel granodiorite (Central Alps, Switzerland) located between the Räterichsbodensee and Grimselsee lakes (Fig. 1a). This shear zone has been selected because (i) the protolith is mineralogically and chemically homogeneous at the outcrop scale, (ii) there is no pre-alpine deformation that could have induced mineral changes and mass transfer and (iii) the chemical and mineralogical evolution is the same whatever the width of the strain gradient (Fourcade *et al.*, 1989; Marquer, 1989). Therefore, changes in mineralogy and bulk chemistry across the strain gradient only reflect variations of parameters related to the alpine deformation (*P*, *T* and mass transfer).

MINERALOGICAL EVOLUTION AND CHEMICAL MASS-TRANSFER

Sixteen samples have been taken along a 100 m wide strain gradient from the weakly deformed granodiorite to the ultramylonitic zone to characterize the simultaneous mineralogical and geochemical evolution. These samples have been subdivided into five groups of compositions: (i) the protolith composition consists of an average of 10 weakly deformed granodiorites, (ii) one orthogneiss (sample A15), (iii) an average of four mylonites (samples AD25, AD22, AD16, A18), and (iv) one ultramylonite (sample AD23a). The fifth sample (v) is a chlorite-bearing ultramylonite, which is in the highest-strain zones of an ultramylonite (0608e). In previous studies (Marquer *et al.*, 1985; Fourcade *et al.*, 1989), chlorite-bearing rocks and assemblages were avoided because they were interpreted as retrograde features. In contrast, in this contribution, chlorite-bearing shear bands are considered as the highest strain zone and most altered rock by metasomatism. Because of its small size, bulk composition was estimated by combining image analysis with in-situ mineral compositions. Consequently, mass transfer has not been quantified in this sample due to the large uncertainty of its composition; therefore, only qualitative results are discussed. Sample names and chemical composition used are presented in Table 1.

Mineralogical evolution

The weakly deformed Grimsel granodiorite, which is considered as the protolith, is characterized by a metastable magmatic assemblage of oligoclase (~An21, 50 vol%), quartz (21 vol%), K-feldspar (14 vol%) and biotite (14 vol%) (Figs 1b & 2a). Magmatic biotite is partially recrystallized into metamorphic biotite (Fig. 2a). With increasing strain intensity, the Grimsel granodiorite progressively evolved into a fine grain albitic mylonite rich in sheet silicates (Fig. 2). In the orthogneiss, magmatic oligoclase is replaced by albite (An02, >45 vol%) with numerous minute inclusions of epidote and white mica (Fig. 2b). Samples qualified as mylonites show minor mineralogical changes with respect to the orthogneiss, except for a general reduction in grain size and a moderate increase in white mica content (Fig. 2c). Albite occurs as 'clean'

© 2012 Blackwell Publishing Ltd

Table 1. Bulk composition of four sets of samples representative of the chemical evolution along the strain gradient in the Grimsel granodiorite. The raws given in mol and mol% are the compositions used for modelling.

	Protolith		Orthogneiss	Mylonite		Ultramylonite	Chl-bearing Ultramylonite
	(n = 10)		A15	AD25 AD22 AD16 A18		AD23a	0608[e]
Density	2.62		2.66	2.72		2.78	–
wt%		1σ st. dev.			1σ st. dev.		
SiO_2	64.98	1.31	64.30	64.46	1.83	65.45	62.43
TiO_2	0.64	0.04	0.61	0.65	0.07	0.65	–
Al_2O_3	16.39	0.62	16.92	16.46	0.15	16.68	16.26
FeO	3.74	0.23	3.67	4.00	0.26	3.39	5.38
MnO	0.09	0.01	0.08	0.09	0.01	0.06	–
MgO	1.12	0.10	0.98	1.58	0.50	2.60	4.08
CaO	2.96	0.24	3.15	2.90	0.30	0.70	0.00
Na_2O	5.06	0.46	5.34	4.95	0.27	3.10	3.33
K_2O	3.20	0.18	2.90	2.94	0.16	4.84	3.59
P_2O_5	0.19	0.02	0.17	0.18	0.02	0.17	–
LOI	0.79	0.17	0.80	1.01	0.25	1.74	4.94
total	99.14		98.92	99.20		99.38	
mol pseudosection							
SiO_2	1.0815		1.0702	1.0728		1.0893	1.0930
Al_2O_3	0.1607		0.1659	0.1614		0.1636	0.1678
FeO	0.0521		0.0511	0.0556		0.0472	0.0787
MgO	0.0277		0.0243	0.0393		0.0645	0.1065
CaO	0.0528		0.0562	0.0518		0.0125	0.0000
Na_2O	0.0816		0.0862	0.0799		0.0500	0.0565
K_2O	0.0339		0.0308	0.0312		0.0514	0.0400
mol% pseudosection							
SiO_2	72.57		72.08	71.91		73.68	70.86
Al_2O_3	10.78		11.18	10.82		11.06	10.88
FeO	3.49		3.44	3.73		3.19	5.10
MgO	1.86		1.64	2.63		4.36	6.90
CaO	3.54		3.78	3.47		0.84	0.00
Na_2O	5.47		5.80	5.36		3.38	3.66
K_2O	2.28		2.07	2.09		3.48	2.60

porphyroblasts free of inclusions (Fig. 2c). Epidote and white mica crystallized preferentially in shear bands around the albite porphyroblasts (Fig. 2c). Due to their heterogeneous nucleation, the amount of white mica and epidote is difficult to estimate but it remains < 10 to 15 vol%. Magmatic K-feldspar is recrystallized and partially albitized. In the orthogneiss and mylonite, shear bands are characterized by a higher amount of white mica. In the ultramylonite (AD20), magmatic phases have been completely recrystallized and the metamorphic albite volume decreases to 30 vol% whereas phengite constitutes up to 30 vol% of the whole rock (Fig. 2d). The ultramylonite is also characterized by an almost complete lack of epidote.

The highest strain zones of the ultramylonite (0608e), are characterized by the local occurrence of a Ca-free assemblage that consists of chlorite in equilibrium with biotite, albite and white mica (Fig. 2e,f). From the undeformed granodiorite to the ultramylonite, the volume of quartz and biotite remains constant but these phases are totally recrystallized into metamorphic phases.

In terms of mineral composition variation along the strain gradient, particular attention is paid to mica because its chemical composition appears to be very sensitive to changes in bulk composition plus white mica is a widely used phase for barometry. Marquer (1987) and Challandes *et al.* (2008) have shown that in this strain gradient, the Si-content in white mica ranges between 3.25 and 3.31 p.f.u. in the orthogneiss, mylonite and ultramylonite. Si-content of phengite from the chlorite-bearing ultramylonite ranges continuously from 3.26 to 3.15 p.f.u with a few analysis *c.* 3.30 p.f.u. (Fig. 3). Biotite shows an increase in XMg with increasing strain, from 0.45 in magmatic biotite in weakly deformed rocks to 0.55 in metamorphic biotite in the ultramylonite (Marquer, 1987). Biotite from the chlorite-bearing ultramylonite shows the same consistent XMg value (0.54–0.55).

Chemical mass transfer

Mass balance calculations have been performed to quantify mass transfer and its effect on phase relations. Ten chemical whole-rock analyses of the Grimsel granodiorite, sampled in a radius of 500 m around the shear zone, have been used to characterize the protolith composition. One sigma standard deviations on each chemical component define the range of the initial composition, interpreted to be magmatic. Bulk compositions are presented in Table 1.

Mass balance results calculated from the statistical approach of Baumgartner & Olsen (1995) are shown in Fig. 4 and in Table 2. Uncertainties on each chemical element in the profile have been calculated with respect to protolith standard deviations. Measured densities are presented in Table 1 and increase by a factor of 1.06 ± 0.05 across the shear zone.

Chemical mass transfers become significant in the mylonite with an enrichment in MgO (+42%, percentage of mass change of a component with respect to the protolith) (Fig. 4a). The ultramylonite shows enrichments in MgO (+132%) and K_2O (+51%) coupled with hydration (H_2O +120%) and losses of CaO, Na_2O, MnO and FeO (−76%, −39%, −33% and −9% respectively) (Fig. 4a). Other elements vary within the range of the initial magmatic heterogeneities and are considered as immobile during the shear zone formation.

The strong relative enrichment in MgO (+132%) in the ultramylonite is commonly used to classify such alteration as a Mg-metasomatism; however, this classification tends to overemphasize the role of MgO in the process of alteration. Calculated absolute mass changes rather suggest that the losses of CaO and Na_2O (−2.28 and −1.98 g 100 g^{-1}, respectively) are larger in magnitude than the gain in MgO (+1.49 g 100 g^{-1}) (Fig. 4b). Deformation and mass transfers occurred at almost constant mass (−1.17 ± 2.33 g) with a small decrease in volume of −6.9 ± 2.2%. A simplified mass-balance equation can be written as:

$$100\text{g Grimsel granodiorite} + 1.49\text{g MgO} + 1.58\text{g } K_2O + 0.93\text{g L.O.I.} \rightarrow 98.83\text{g Ultramylonite} + 0.44\text{g } Fe_2O_3 + 0.03\text{g MnO} + 2.28\text{g CaO} + 1.98\text{g } Na_2O.$$

© 2012 Blackwell Publishing Ltd

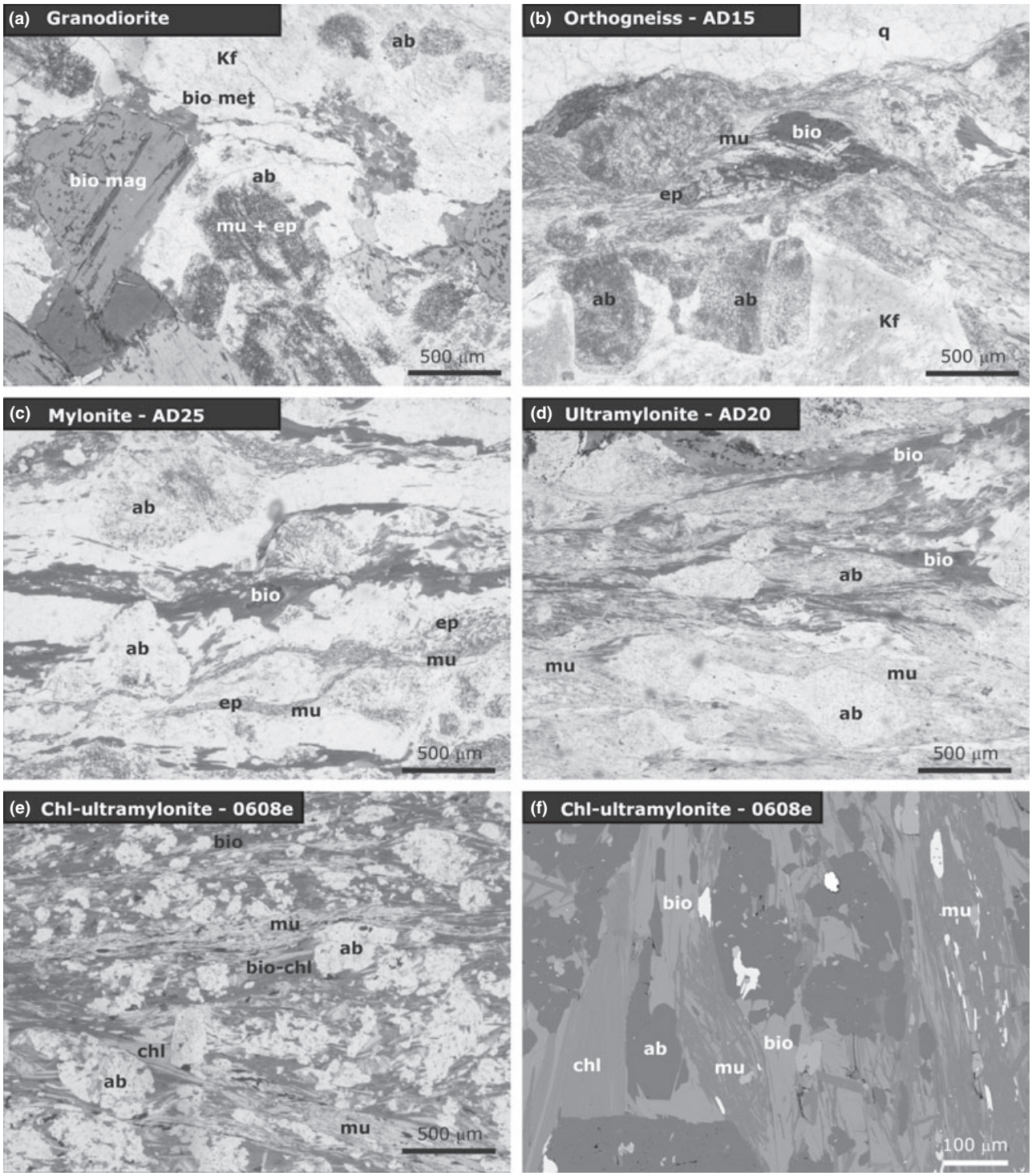

Fig. 2. Representative textures and assemblages observed along the strain gradient. (a) Protolith showing the magmatic texture and mineralogy. Magmatic oligoclase is already replaced here by albite + epidote and phengite. (b) Orthogneiss showing rare relicts of K-feldspar with large amounts of metamorphic albite. White mica occurs as small, unoriented inclusions associated with epidote in the albite porphyroblast. Epidote can be observed throughout the orthogneiss as small porphyroblasts (< 200 μm). (c) Mylonite showing the complete recrystallization of magmatic phases into metamorphic minerals. Albite occurs as porphyroblasts free of inclusions. Epidote is concentrated in shear bands with white mica. (d) Ultramylonite showing the development of large amounts of white mica in equilibrium with albite. Magmatic K-feldspar is no more present while metamorphic epidote is rare. (e) Ultramylonite showing the local development of chlorite-bearing assemblages in equilibrium with albite, biotite and phengite. (f) Backscattered images of the texture and assemblages in the chlorite-bearing ultramylonite. See location in Fig. 2e. This BSE image has been used to estimate the bulk composition of the chlorite-bearing domains.

© 2012 Blackwell Publishing Ltd

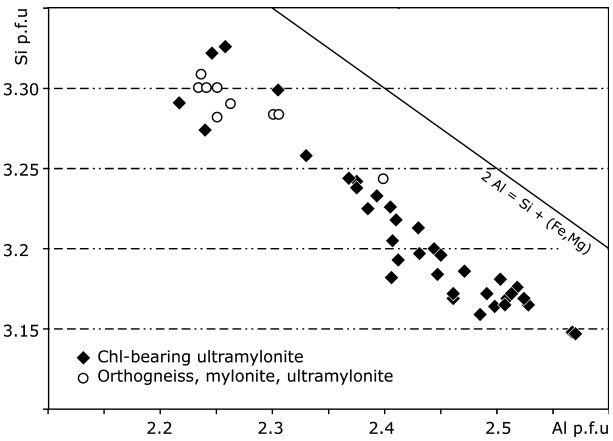

Fig. 3. Composition of white mica measured in a chlorite-bearing ultramylonite (black diamonds) showing a continuous range in Si content per formula unit (p.f.u) between 3.33 and 3.15. White circles correspond to phengite in the orthogneiss, mylonite and ultramylonite (see Marquer, 1987 and Challandes *et al.*, 2008).

The bulk composition for the chlorite-bearing domains in the highest-strain rock is based on the following mineralogical compositions inferred from image analysis: 28% albite, 21% phengite, 18% biotite, 11% chlorite and 22% quartz. Chlorite domains are obviously characterized by a complete loss of CaO as indicated by the lack of Ca-bearing phases. Qualitative mass changes are consistent with the trend observed in the ultramylonite including a strong enrichment in MgO (>250%) and a loss of Na_2O (~40%). With our estimated bulk composition K_2O would be immobile with respect to the protolith.

Although metasomatism may depend upon the composition and amount of infiltrating fluid, composition of the protolith and *P–T* conditions, it appears that gain of MgO coupled with losses of CaO and Na_2O are common features for metasomatized quartzo-feldspathic rocks in ductile shear zones (Table 3). The compilation of Table 3 raises several questions related to metasomatism in shear zones: what controls the nature of mass transfer in shear zones? Is fluid composition the most critical variable? Do metamorphic reactions play a significant role in the nature and quantity of mass transfer? Why are CaO/Na_2O losses commonly coupled with MgO gain?

THERMODYNAMIC MODELLING OF OPEN SYSTEMS

A series of computed phase diagram projections and sections are used to constrain the *P–T* of deformation and mass transfer and to investigate the influence of mass transfer on phase relations. For this purpose the model system Na_2O–CaO–K_2O–FeO–MgO–Al_2O_3–SiO_2–H_2O was chosen to calculate phase relationships using Perple_X'07 software (Connolly, 2005) with the thermodynamic database of Holland & Powell (1998, as revised in 2002). Solution models and end-member phases considered in the modelling are listed in Table 4. Bulk compositions used in these models have been obtained by whole rock XRF analyses given in Table 1, except for the chlorite-bearing ultramylonite, which is an estimated bulk rock composition.

P–T diagrams

P–T sections have been calculated for the weakly deformed granodiorite, mylonite, ultramylonite and chlorite-bearing ultramylonite compositions to refine the *P–T* conditions of the deformation and evaluate the influence of mass transfer on the phase diagram topology (Fig. 5). In applying *P–T* sections, we make the implicit assumption of local equilibrium at the scale of the rock analysed by XRF (i.e. tens of cm^3). Although chemical potential gradients may exist along the 100 m wide strain gradient between the metastable host-rock and the equilibrated highest strain zone, it is assumed that these gradients can be neglected on the scale of the sample. All the diagrams have been calculated using water saturated conditions.

The *P–T* section calculated for the granodiorite composition (Fig. 5a) shows that the magmatic assemblage is stable in a large multivariant field on the low pressure and high temperature side of the diagram that consists of pl, q, kf, bio with minor garnet (the predicted amount is <2 vol%). The metamorphic assemblage mu-bio-ep-ab-q-kf is stable in a relatively large *P–T* field below 9 kbar and 510°C. Comparison of measured Tschermak substitution in phengite (Si = 3.25–3.31 p.f.u.) with calculated isopleths suggests that the pressure conditions of deformation range between 5.1 and 7.4 kbar assuming temperatures of 425–475°C (average of 6.2 ± 1 kbar for 450°C ± 25°C; the temperature of 450°C is taken from Challandes *et al.* (2008)). The section calculated with the orthogneiss composition is not presented but gives similar results.

In the mylonite, a gain of 50% of MgO does not alter significantly the topology of the *P–T* section (Fig. 5b). *P–T* conditions for this rock have been estimated at 6.3 ± 1 kbar for 450°C ± 25°C.

The *P–T* section calculated with the ultramylonite composition shows some significant differences (Fig. 5c): (i) white mica is stable in the entire *P–T* range while it is restricted to the HP-LT side of the protolith and mylonite diagram, (ii) the stability field of K-feldspar is reduced, (iii) the stability field of epidote-bearing assemblages is expanded to HP–LT conditions and (iv) chlorite-bearing assemblages become stable on the LT-side of the diagram. The metamorphic assemblage mu-bio-ep-ab-q observed in the ultramylonite is stable from 310–370 °C at 4 kbar to 430–530 °C at 10 kbar. Phengite compositions measured in the ultramylonite (Si = 3.25–3.30 p.f.u.) suggest *P–T* conditions of deformation of 5–7.1 kbar and 425–475°C (average of 6.5 ± 0.5 kbar for 450°C ± 25°C).

© 2012 Blackwell Publishing Ltd

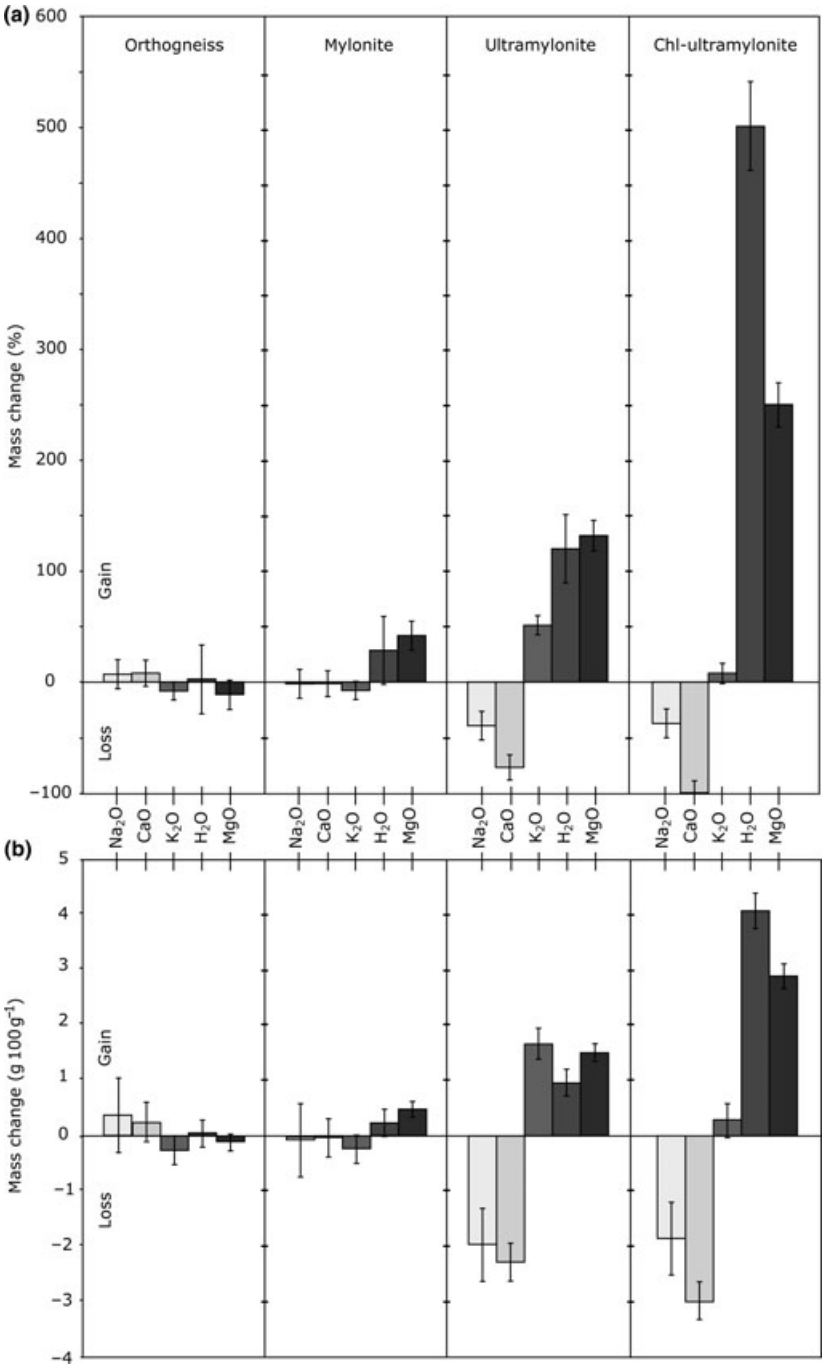

Fig. 4. (a) Relative mass transfer along the strain gradient. (b) Absolute mass change given in g $100g^{-1}$.

Because intense metasomatism (complete loss of CaO and gain of MgO) the section calculated with the chlorite-bearing ultramylonite has a completely different topology (Fig. 5d). Almost the entire range of the *P–T* conditions is characterized by the stability of chl-bio-mu-ab-q. The Si-content of phengite measured in the chlorite-bearing assemblage varies continuously from 3.30 to 3.15. Based on the *P–T* conditions estimated along the strain gradient (6.5 kbar, 450°C) we suggest that only phengite with a low Tschermak component (~3.15–3.20) is in equilibrium with chl-bio-ab-q.

P–T conditions of the five samples are consistent suggesting that the deformation was isobaric and isothermal. For the following discussion, our preferred *P–T* conditions for deformation and mass transfer are 450°C and 6.5 kbar which are in good agreement with those suggested by Challandes *et al.* (2008).

The effect of mass transfer at the *P–T* conditions of interest can also be shown in Fig. 6 and Table 5

© 2012 Blackwell Publishing Ltd

Table 2. Predicted mineralogical composition of five samples from the strain gradient. Measured modes and strain intensity (ϵs) are from Marquer (1987): protolith – AD26, orthogneiss – average of AD13 and AD3; mylonite – AD19; ultramylonite – AD23. The predicted mineralogical composition are derived from *P–T* sections calculated with the compositions of Table 2 (see section modelling for more details).

	Absolute mass change ($g\ 100g^{-1}$)						Relative mass change (%)					
	Orthogneiss		Mylonite		Ultramylonite		Orthogneiss		Mylonite		Ultramylonite	
		1σ		1σ		1σ		1σ		1σ		1σ
SiO_2	0.23	2.33	−0.18	2.32	0.46	2.40	0.4	3.6	−0.3	3.6	0.7	3.7
TiO_2	−0.02	0.06	0.01	0.06	0.01	0.06	−3.3	9.1	2.1	9.1	1.5	9.1
Al_2O_3	0.78	0.96	0.16	0.95	0.29	0.96	4.7	5.8	1.0	5.8	1.7	5.8
FeO	−0.02	0.34	0.28	0.34	−0.35	0.34	−0.5	9.0	7.5	9.0	−9.4	8.9
MnO	−0.01	0.01	0.00	0.01	−0.03	0.01	−9.9	15.9	0.5	15.9	−33.4	15.8
MgO	−0.13	0.15	0.47	0.15	1.49	0.15	−11.3	12.9	41.8	13.0	132.1	13.7
CaO	0.24	0.35	−0.04	0.35	−2.28	0.34	7.9	11.8	−1.5	11.7	−76.4	11.5
Na_2O	0.36	0.67	−0.08	0.67	−1.98	0.66	7.0	13.1	−1.7	13.1	−38.8	12.9
K_2O	−0.26	0.27	−0.25	0.26	1.65	0.28	−8.1	8.2	−7.6	8.2	51.2	8.7
P_2O_5	−0.02	0.03	−0.01	0.03	−0.02	0.03	−9.3	15.1	−4.8	15.1	−10.6	15.0
L.O.I.	0.02	0.24	0.23	0.24	0.96	0.25	2.7	30.7	28.5	30.6	120.2	30.8

Table 3. Compilation of previous studies of chemical mass transfer in shear zones affecting metagranites.

Reference	Locality	Protolith	Metamorphic facies	Chemical mass transfer: Gain	Chemical mass transfer: Loss
Rossi *et al.* (2005)	Mont-Blanc (France)	Granite	Greenschist	Fe, Ca	K
				Si	Ca, Na, K
				Mg	Si, Ca, Na, K
Yonkee *et al.* (2003)	Sevier orogenic belt (Utah)	Granitic gneiss	Greenschist	Mg	Na, Ca, K
Bialek (1999)	Lusatian Massif, Poland	Granodiorite	Greenschist	Ca, Mn	Na
Hippert (1998)	Sao Francisco craton (Brazil)	Granitic gneiss	Greenschist	Mg, Fe	Ca, Na
Glodny & Grauert (2009)	Schwarzwald (Germany)	Quartzdioritic gneiss	Lower greenschist	K	Ca, Na
Sassier *et al.* (2006)	Ile d'Yeu (France)	Granitic gneiss	Amphibolite	Mg, K	Ca, Na
Selverstone *et al.* (1991)	Tauern Window (E Alps)	Granodiorite	Eclogite/amphibolite	Al, Mg, Fe	Si, Ca, Na
Keller *et al.* (2004)	Monte Rosa nappe (W Alps)	Granite	Eclogite	Si	Al, K
Demény *et al.* (1997)	Sopron-Fertőrákos (E Alps, Hungary)	Granite	Eclogite	Mg	Na, Ca, Fe
				Si, Mg	Na, Ca, K, Fe
Challandes (2001)	Suretta Nappe (Central Alps)	Rhyolite	Blueschist	Mg	Na, Ca

Table 4. Solid solutions model and phases used in the sections.

Phases	Solid solution label used in PerpleX	Solid solution label used in the text	Independent end-members	References
Biotite	Bio(HP)	bio	Annite–phlogopite–eastonite	Holland & Powell (1998)
Chlorite	Chl(HP)	chl	Clinochlore–daphnite–amesite–Al-free chlorite	Holland & Powell (1998)
Garnet	Gt(WPH)	Gt	Almandine–pyrope–grossular	White *et al.* (2007)
K-feldspar	San	Kf	Sanidine–albite (high order)	Waldbaum & Thompson (1969)
Plagioclase	Pl(h)	Pl	Anorthite–albite	Newton & Haselton (1981)
White mica	Mica(CH1)	mu	Muscovite–celadonite–paragonite–margarite–Fe-celadonite	Coggon & Holland (2002)
Clinozoisite	cz	Cz		
Quartz	q	Q		
Sillimanite	sil	Sil		
Kyanite	ky	Ky		

where the modal abundance evolution is reported as a function of strain and therefore mass transfer. Modes were calculated for the five samples at 450°C and 6.5 kbar. Equilibration of the metastable magmatic assemblage at metamorphic conditions induces the complete breakdown of magmatic plagioclase into albite + epidote and the appearance of white mica coupled with the minor breakdown of K-feldspar. The observation of relicts of K-feldspar porphyroclasts and magmatic biotite suggests that the equilibration remains partial. Stable assemblages predicted in the orthogneiss are not significantly different than the equilibrated protolith because the strain observed in the orthogneiss occurred under closed system conditions (the minor changes visible in Fig. 6 are interpreted as magmatic heterogeneities rather than

© 2012 Blackwell Publishing Ltd

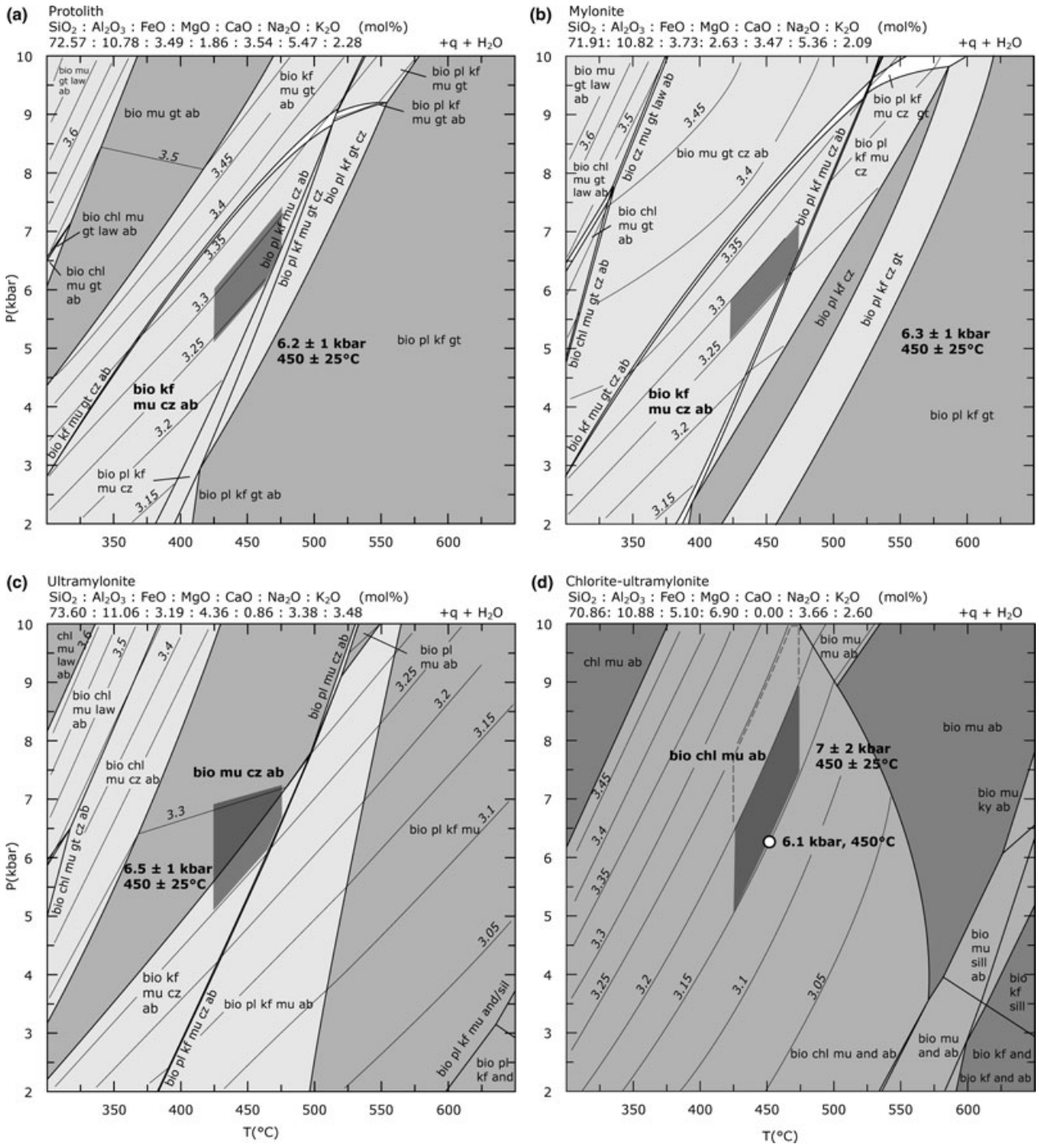

Fig. 5. *P–T* sections calculated for (a) the protolith composition and (b) the mylonite, (c) the ultramylonite and (d) the chlorite-bearing ultramylonite composition in the NaCaFMASH system under water saturated conditions. Si content per formula unit in white mica is contoured on all diagrams. The preferred *P–T* conditions of deformation correspond to the coloured domain. *P–T* conditions are given by the stable assemblage observed and the Si-content in phengite assuming a temperature of 450 ± 25°C (Challandes *et al.*, 2008).

the result of metasomatism). Under open system conditions in the mylonite, ultramylonite and chlorite-bearing ultramylonite, the white mica content increase is correlated with the breakdown of K-feldspar, albite and epidote (Fig. 6). Crystallization of chlorite in the highest strained sample is associated with the breakdown of biotite, white mica and minor epidote.

© 2012 Blackwell Publishing Ltd

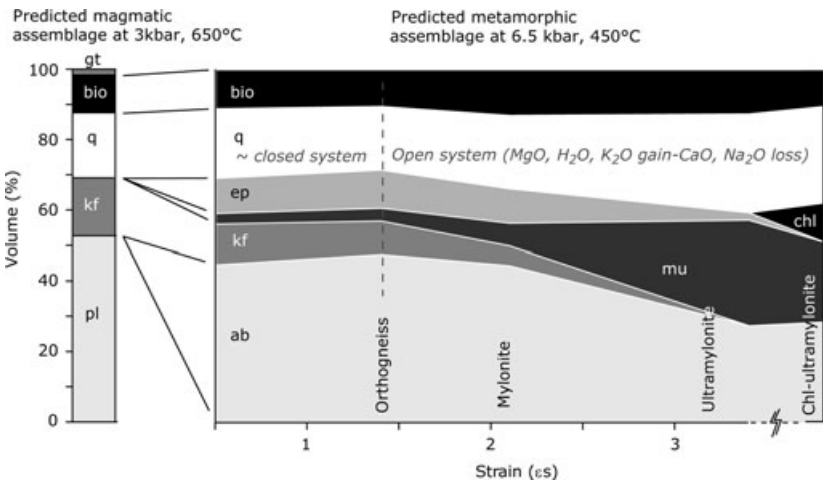

Fig. 6. Predicted mineralogical evolution estimated at 6.5 kbar and 450°C using the four bulk composition presented in Table 2. For more details, see the modelling section. The magmatic assemblage has been estimated using the protolith composition at 3 kbar, 650°C, which may correspond to the Variscan *P–T* conditions of emplacement and crystallization of the granodioritic magma.

Table 5. Calculated modes (vol%) and CaO, MgO content (wt%) calculated with the chemical potential section of Fig. 10

	Magmatic	Metamorphic			
	650°C – 3kbar	450°C – 6.5 kbar			
	Protolith	Orthogneiss	Mylonite	Ultramylonite	Chl-ultramylonite
εs	0	1.4	2.1	3.4	–
bio	11	10	13	12	11
pl	52	0	0	0	0
ab	0	48	45	28	29
kf	17	9	6	0	0
mu	0	4	6	30	22
ep	0	11	10	2	0
chl	0	0	0	0	11
q	19	18	21	28	27
gt	2	0	0	0	0

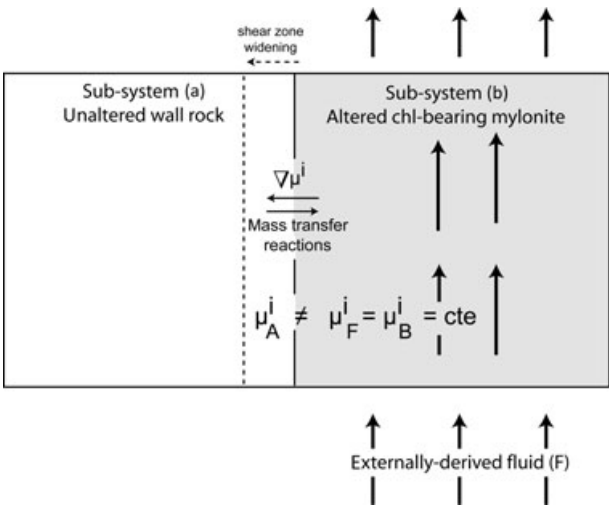

Fig. 7. Conceptual model of the shear zone. It consists of two sub-systems A and B that correspond to the unaltered host granite and the altered chlorite-bearing ultramylonite, respectively. We assume that both systems are in local equilibrium. The contact is characterized by chemical potential gradients that equalized by metamorphic/metasomatic reactions and diffusion of component down chemical potential gradient in a static fluid between the chlorite-bearing ultramylonite (B) and the metastable wall-rock (A). Orthogneiss, mylonite and ultramylonite are formed during this process of equilibration.

Modelling of open-system: quantitative chemical potential diagrams

The reactions involved in the shear zone development and quantification of mass transfer has been thermodynamically modelled using isobaric-isothermal phase diagram projections and sections as a function of the chemical potentials (μ) of the mobile components (MgO, CaO & Na_2O). The choice of the determinative variables is dictated by our conceptual model of shear zone widening described below.

The first stage of shear zone formation (Fig. 7) corresponds to its nucleation on a pre-existing or newly formed crack, which is assumed to be the locus of intense fluid infiltration and metasomatism with the formation of the chlorite-bearing assemblage. The second stage corresponds to shear zone widening and formation of the orthogneiss, mylonite and ultramylonite that compose the metre-scale strain gradient. At the end of the nucleation stage, we suggest that the shear zone is a system in disequilibrium that can be divided in two end-member sub-systems where local equilibrium is applicable (Fig. 7). The first sub-system (A) corresponds to the metastable unaltered and weakly deformed granodiorite. During the widening stage, sub-system (A) is assumed to be water saturated with a nearly static pore fluid where dissolved species are transported by diffusion orthogonal to the shear zone. Sub-system (B) is the metasomatized chlorite-bearing assemblage that was formed as a consequence of intense infiltration dominated metasomatism. Within each sub-system, equilibrium implies that the chemical potential of each component is equalized and determined by the *P–T* conditions and bulk rock composition. However at a larger scale, the chlorite-bearing ultramylonite (B) and the metastable magmatic granodiorite (A) are in disequilibrium with

© 2012 Blackwell Publishing Ltd

each other and the interface between these two systems is characterized by chemical potential gradients. To reach equilibrium, the chemical potential gradients must be eliminated by metamorphic/metasomatic reactions and diffusion of components through the pore fluid. We suggest that intermediate rocks (orthogneiss, mylonite and ultramylonite) are formed during the process of equilibration of the metastable magmatic assemblage towards the chlorite-bearing ultramylonite via diffusion metasomatism, and represent various degree of re-equilibration.

Chemical potential phase diagrams are the most appropriate diagrams to model the formation of these intermediate rocks. The effect of K_2O mobility on phase relations is not discussed. For consistency, all of the calculated μ-μ diagrams use gained components on the x-axis (MgO) and lost components on the y-axis (CaO or Na_2O).

Phase relations are introduced with μMgO–μCaO and μMgO–μNa_2O projections in simplified chemical systems, K_2O–Al_2O_3–MgO–CaO and K_2O–Al_2O_3–MgO–Na_2O respectively, with quartz and H_2O in excess. Only pure end-members are considered (K-feldspar, muscovite, phlogopite, clinochlore, kaolinite with zoisite, grossular or albite). Modelling has also been performed in a more realistic chemical systems (CaO–Na_2O–K_2O–FeO–MgO–Al_2O_3–SiO_2 with saturated H_2O) that take into account the effect of solid solutions (Table 4). In addition, phase diagram sections were computed with the amount of immobile components (K_2O–FeO–Al_2O_3–SiO_2) fixed. Because only two mobile components can be considered in a 2D phase diagram, first Na_2O and then CaO are fixed in the μMgO–μCaO and μMgO–μNa_2O sections respectively.

P–T sections for the five samples (Fig. 5) are used to compute the chemical potential of all components, including the mobile components that are assumed to diffuse during the equilibration process. Knowing these values, it is possible to determine gradients in chemical potential and therefore determine the probable direction of diffusion mass transfer that will be compared with observations.

Chemical potential projections

The μMgO–μCaO and μMgO–μNa_2O projections presented in Fig. 8, are calculated at 450°C and 6.5 kbar. These diagrams show that the assemblages K-feldspar + clinozoisite and K-feldspar + albite are restricted to the high values of μCaO and μNa_2O respectively and low values of μMgO (Fig. 8). A decrease in CaO or Na_2O chemical potential (at constant μMgO) induces the stabilization of muscovite via the reactions:

$$2/3\text{cz} + 1\text{kf} + 2/3\text{H}_2\text{O} = 1\text{mu} + 2\text{q} + 4/3\text{CaO} \quad (1)$$

$$2\text{ab} + 1\text{kf} + 1\text{H}_2\text{O} = 1\text{mu} + 6\text{q} + 1\text{Na}_2\text{O} \quad (2)$$

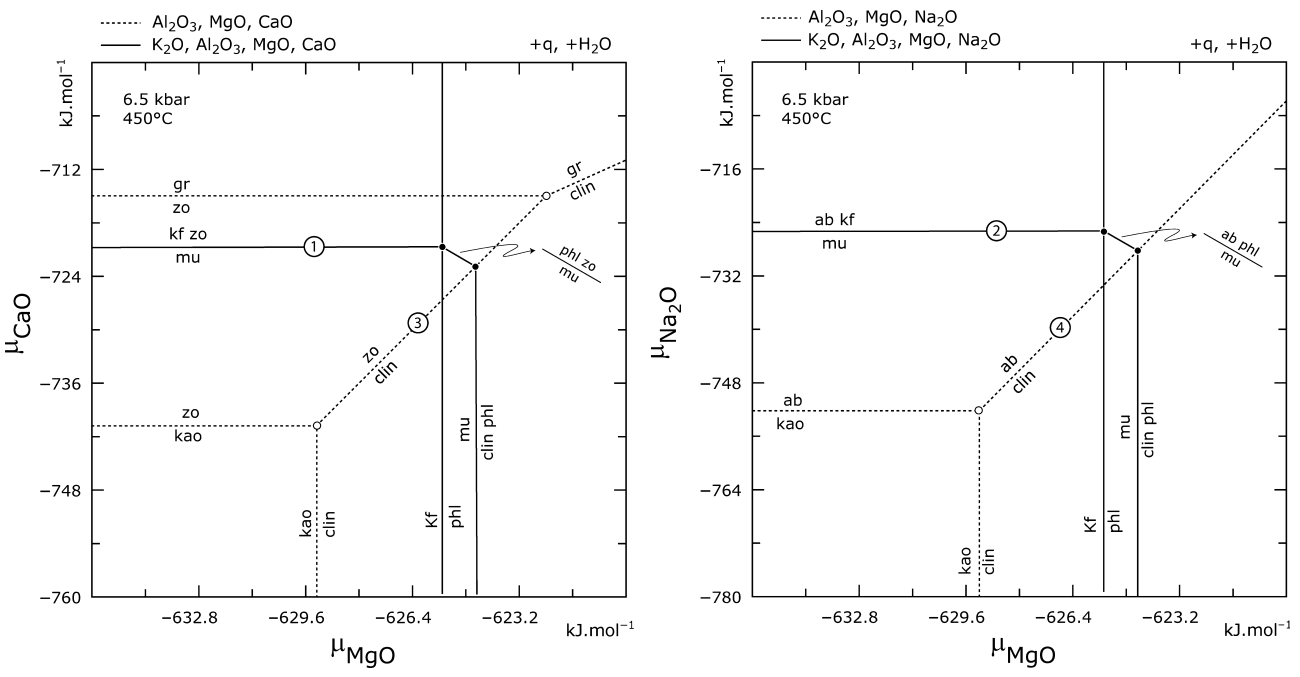

Fig. 8. Quantitative μCaO–μMgO and μNa_2O–μMgO projections calculated at 450°C and 6.5 kbar at water-saturated conditions. Solid lines correspond to univariant reactions in the K_2O–Al_2O_3–MgO–CaO/Na_2O system, whereas dashed lines are univariant reactions belonging to the sub-system Al_2O_3–MgO–CaO/Na_2O. Circled numbers correspond to the reaction label used in the text. Phase relations in these simplified systems show that the breakdown of kf-zo and kf-ab (i.e. the metamorphic assemblage observed in the orthogneiss) into a mu-clin assemblage (i.e. ultramylonitique) requires an increase of μMgO coupled with a decrease in μCaO and mNa_2O.

© 2012 Blackwell Publishing Ltd

These reactions result in a K-feldspar + muscovite or clinozoisite/albite + muscovite assemblage depending on the bulk rock composition. The stability of clinozoisite and albite is limited to the high μMgO by two univariant reactions producing clinochlore:

$$1\text{cz} + 3/2\text{q} + 11/2\text{H}_2\text{O} + 15/2\text{MgO} = 3/2\text{clin} + 2\text{CaO} \quad (3)$$

$$1\text{ab} + 2\text{H}_2\text{O} + 5/2\text{MgO} = 1/2\text{clin} + 3/2\text{q} + 1/2\text{Na}_2\text{O} \quad (4)$$

The stable assemblage just below reactions (3) and (4) can be either K-feldspar + muscovite or clinochlore + muscovite. With increasing μMgO, K-feldspar and muscovite are breakdown into phlogopite and clinochlore + phlogopite, respectively.

These phase diagram projections suggest that the sequence of mineralogical changes can be interpreted as the consequence of a decrease in μCaO and μNa$_2$O followed by an increase in μMgO in the shear zone (Fig. 8). This variation in chemical potential also induces a loss of CaO and Na$_2$O with a gain in MgO and H$_2$O in good agreement with the mass balance calculation.

Chemical potential sections

Sections μMgO–μCaO and μMgO–μNa$_2$O (Fig. 9) have been calculated at the same *P–T* conditions (450°C and 6.5 kbar) with the 'partial' unaltered granodiorite composition (Table 2) with a more restricted range of chemical potentials than the projections. The sections in Fig. 9 are characterized by the occurrence of three univariant equilibria, almost independent of μMgO, that separate divariant fields: biotite + k-feldspar + garnet + albite + quartz, biotite + muscovite + clinozoisite + albite + quartz, and biotite + muscovite + chlorite + clinozoite/albite + quartz. The breakdown of the K-feldspar + clinozoite + albite assemblage into muscovite occurred via the univariant reactions:

$$\text{kf} + \text{cz} + \text{bio} + \text{H}_2\text{O} + \text{MgO} = \text{mu} + \text{q} + \text{ab} + \text{CaO} \quad (5)$$

$$\text{kf} + \text{ab} + \text{bio} + \text{cz} + \text{H}_2\text{O} + \text{MgO} = \text{mu} + \text{q} + \text{Na}_2\text{O} \quad (6)$$

These reactions imply a decrease in μCaO and μNa$_2$O with or without increase in μMgO. The stability of chlorite-bearing assemblages is at the lowest μCaO and μNa$_2$O and is limited by the univariant equilibria:

$$\text{cz} + \text{bio} + \text{ab} + \text{H}_2\text{O} + \text{MgO} = \text{chl} + \text{mu} + \text{q} + \text{CaO} \quad (7)$$

$$\text{ab} + \text{bio} + \text{cz} + \text{H}_2\text{O} + \text{MgO} = \text{chl} + \text{mu} + \text{q} + \text{Na}_2\text{O} \quad (8)$$

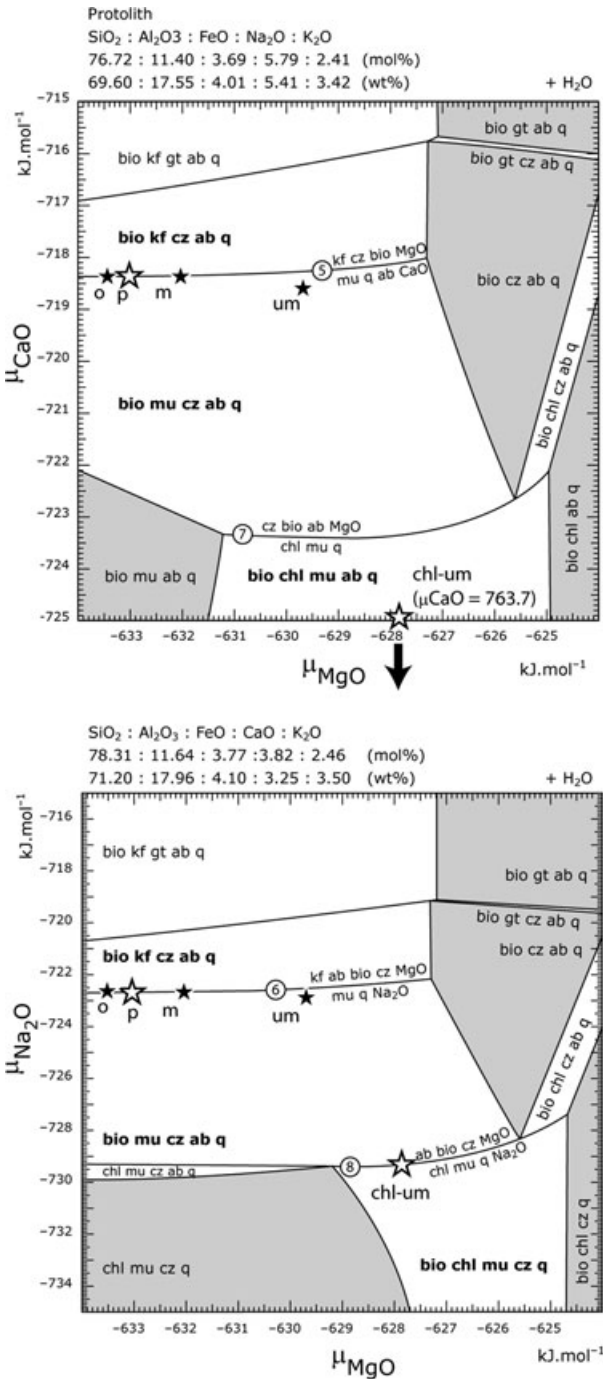

Fig. 9. Quantitative μCaO–μMgO and μNa$_2$O–μMgO section calculated at 450°C and 6.5 kbar for the unaltered granodiorite composition at water-saturated conditions. The white-filled star correspond to the chemical potential value of CaO, Na$_2$O, MgO calculated at 6.5 kbar and 450°C of the tri-variant assemblage kf-cz-mu-bio-ab-q for the unaltered granodiorite composition under a closed-system conditions. Black stars are the chemical potential values for the orthogneiss (o), mylonite (m), ultramylonite (um) and chlorite-bearing ultramylonite (chl-um).

© 2012 Blackwell Publishing Ltd

Table 6. Chemical potential values calculated for each component.

	Chemical potential (kJ mol^{-1})					
	3 kbar, 650°C	6.5 kbar, 450°C				
P–T conditions	Protolith	Protolith	Orthogneiss	Mylonite	Ultramylonite	Chlorite–ultramylonite
SiO_2	−899.089	−870.749	−870.749	−870.775	−870.749	−870.752
Al_2O_3	−1692.910	−1630.090	−1630.070	−1630.200	−1629.820	−1623.280
FeO	−315.226	−295.316	−295.098	−295.962	−297.997	−296.111
MgO	−645.658	−633.068	−633.502	−632.062	−629.700	−627.891
CaO	−728.260	−718.371	−718.380	−718.330	−718.572	−762.314
Na_2O	−756.421	−722.709	−722.721	−722.669	−722.976	−729.529
K_2O	−834.823	−791.952	−791.964	−791.923	−792.857	−810.662

Chemical potentials of CaO, Na_2O and MgO at 6.5 kbar and 450°C for the five samples have been extracted from the corresponding sections (Fig. 5). Values are reported in Table 6 and in the chemical potential sections (see stars in Fig. 9). The stable assemblage predicted at 6.5 kbar and 450°C for the protolith, orthogneiss, and mylonite is biotite + K-feldspar + muscovite + epidote + albite + quartz. This assemblage is trivariant in a chemically closed system, but in a system with two mobile components (MgO and CaO or MgO and Na_2O) it is univariant and corresponds to equilibria (5) and (6) (Fig. 9). The ultramylonite, characterized by the absence of K-feldspar, is located in the divariant field biotite + muscovite + epidote + albite + quartz at higher μMgO and lower μCaO than for the less deformed samples. The chlorite-bearing ultramylonite (sub-system B) is stable at lower chemical potentials for CaO and Na_2O (Fig. 9). With fluid rock interactions, the divariant assemblage biotite + muscovite + chlorite + albite + quartz became Ca-free in the chlorite-bearing ultramylonite. CaO is thus viewed as a perfectly mobile component (as defined by Korzhinskii, 1970) with its chemical potential controlled by the externally-derived fluid. Other mobile components (MgO and Na_2O) have their chemical potential controlled by fluid-rock interactions and more precisely by rock-dominated diffusion.

In the sections in Fig. 9, orthogneiss, mylonite and ultramylonite are interpreted as intermediate stages formed during the process of equilibration of the two sub-systems A (protolith) and B (chlorite-bearing ultramylonite). Therefore, mass transfer and reactions involved during the equilibration of the protolith toward the conditions of the chlorite-bearing ultramylonite is expected to lie on a path between the conditions of these sub-systems (black arrow in Fig. 10). To estimate the amount of CaO, Na_2O and MgO transported in and out the system along the chemical potential path, the μ-μ sections are contoured for the amounts of the mobile components, which are also converted into relative gain or loss with respect to the unaltered granodiorite composition (only the μMgO–μCaO example is shown in Fig. 10a,b). Before equilibration, the granodiorite is composed of 3.39, 1.17 and 0.77 wt% for CaO, MgO and H_2O respectively (calculated values from Fig. 6a, H_2O is taken into account in the normalization). The modal composition of the unaltered and equilibrated granodiorite is albite (45%), quartz (20%), biotite (11%), K-feldspar (11%), epidote (10%) and white mica (3%).

The first stage of the equilibration path corresponds to the evolution of the chemical potential of CaO and MgO along the univariant equilibria (5) towards high μMgO values until K-feldspar is entirely consumed (Fig. 10a,b). This first stage of equilibration induces the crystallization of 12 vol% white mica at the expense of K-feldspar and half of the initial epidote content. The computed phase equilibria indicate that this reaction induces a relative gain in MgO of 144% and H_2O of 80% coupled with a loss in CaO of 48%, assuming no changes in volume and density (Fig. 10-a,b). The modified bulk composition after the complete breakdown of K-feldspar is MgO = 2.86 wt%, CaO = 1.77 wt% and H_2O = 1.39 wt%, which is consistent with observations.

Once K-feldspar has been entirely consumed, the system evolves across the divariant field biotite + muscovite + epidote + albite + quartz towards the chlorite-bearing ultramylonite conditions until it intersects the univariant reaction (7) and (8) where chlorite is produced. During this second stage, epidote reacts with albite, quartz and minor biotite to produce an additional gain of 1.5 vol% of white mica. The reaction along the μ-μ path requires a loss of 66% of the initial CaO content and also minor loss of MgO with respect to the end of the first stage of equilibration (133% *v.* 144% total gain respectively). To keep the system water-saturated, an extra gain of 1.5 wt% of water is required at the end of stage 2.

The last stage of equilibration corresponds to the formation of chlorite. When the chemical potential path intersects the univariant reaction (7), the remaining epidote (3 vol%) reacts with biotite and minor albite to produce 3 vol% of chlorite with an extra gain of 4 vol% of white mica. The rock is at that stage composed of albite (44%), quartz (23%) white mica (17%), biotite (12%) and chlorite (3%). When all the epidote is consumed, the system becomes CaO-free and the rock is slightly enriched in MgO with respect to the end of stage 2 (+139% of the initial content). The chemical potential of the CaO and Na_2O will

© 2012 Blackwell Publishing Ltd

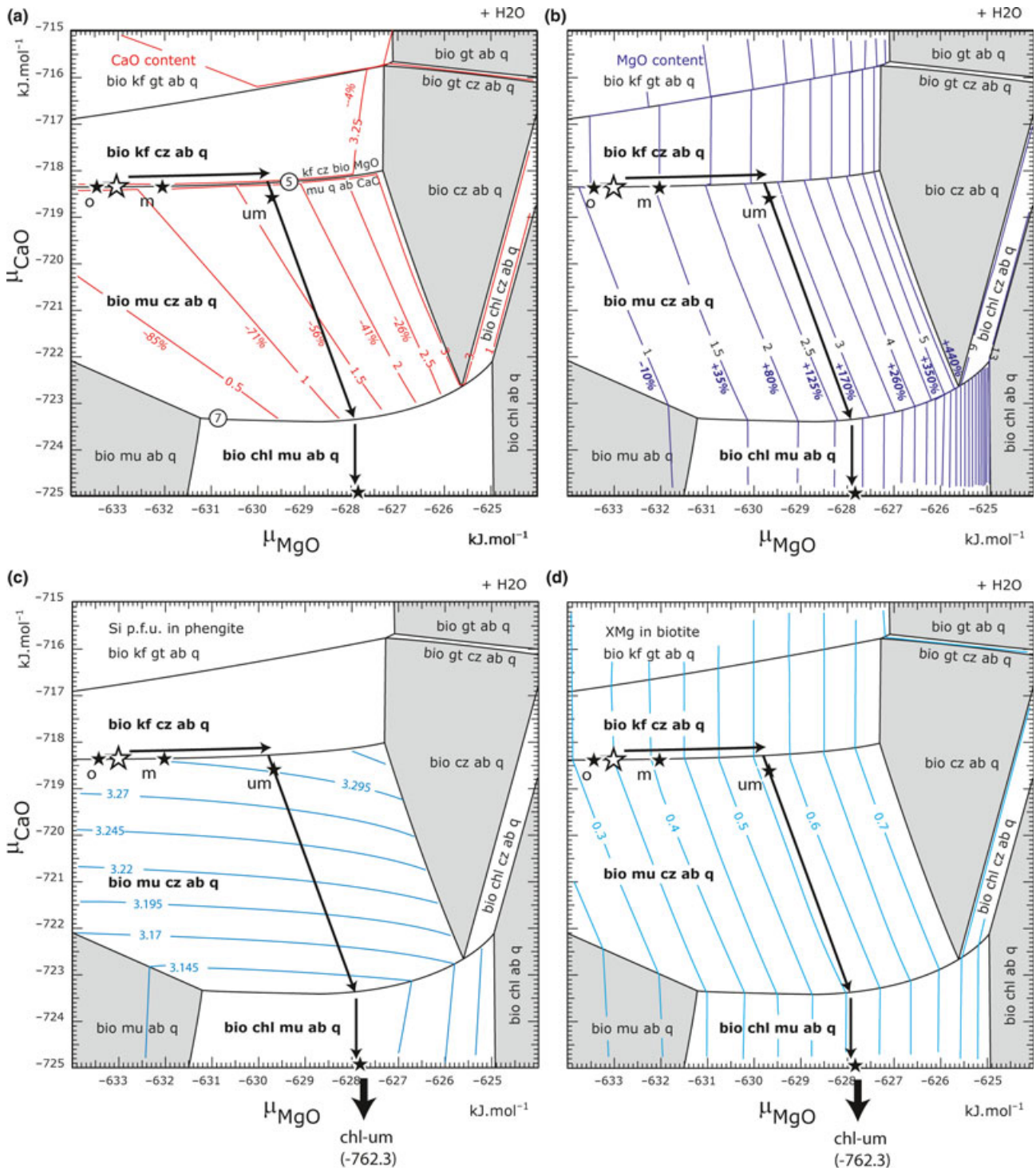

Fig. 10. Quantitative μCaO-μMgO section calculated at 450°C and 6.5 kbar for the unaltered granodiorite 'partial' composition at water-saturated conditions contoured for (a) CaO content of the system, (b) MgO content of the system. Numbers on the isopleth are expressed in wt% while those located on the side of the isopleths correspond to the relative mass change expressed in wt% with respect to the initial content of CaO (3.39 wt%) and MgO (1.13 wt%). The equilibration chemical potential path is represented as an arrow. (c) Section contoured for Si-content p.f.u in white mica. (d) Contours of XMg in biotite.

be buffered by the univariant assemblage (7) and (8) until epidote and albite respectively are completely exhausted. In this case, epidote is the limiting reactant and the rock path leaves the reaction and moves across the divariant field biotite + muscovite + chlorite + albite + quartz to a lower chemical potential of CaO

© 2012 Blackwell Publishing Ltd

(Fig. 10a,b). The last part of the equilibration path, evolution at constant μMgO to lower values of μCaO, does not induce changes in mineralogy and chemistry (Fig. 10a,b).

The computed phase equilibria shows that the most significant changes in terms of chemistry and mineralogy occur during the first stage of equilibration corresponding to the formation of the ultramylonite via the breakdown of K-feldspar and epidote into white mica. The following stages that induce the crystallization of white mica and chlorite have a minor impact on the petrography of the rock. Although the CaO and MgO mass transfer and modal evolution estimated with the μMgO-μCaO section are consistent with the observations, it should be remembered that the phase equilibria computations were done for fixed Na_2O content. We have performed the same type of computation with μMgO-μNa_2O sections, keeping CaO constant. In this calculation, the loss of Na_2O due to the breakdown of albite via reactions (6) and (8) is associated mainly with crystallization of phengite and gain in MgO (Fig. 9). Therefore, the amounts of white mica and MgO estimated from the μMgO-μCaO section are considered to be minimum estimates.

In multicomponent systems, the chemical potential of a component is not a direct measure of its concentration. Hence, the slope and distribution of CaO content isopleths varies significantly across the μ-μ diagram (Fig. 10a). While a decrease in μCaO in the divariant field biotite–K–feldspar–epidote–albite–quartz has no effect on the CaO concentration, a comparable decrease in the divariant field biotite–muscovite–epidote–albite–quartz may cause either a decrease or increase in CaO depending on the variation in μMgO (Fig. 10a).

Implications for mineral composition

The chemical potential path also has a strong influence on mineral composition (Connolly, 1990). The μMgO–μCaO section has been contoured for the Si content of white mica per formula unit (p.f.u.) (Fig. 10c). The phase diagram section shows that along the first part of the inferred equilibration path, white mica produced by the breakdown of K-feldspar + epidote + albite via reaction (5) and (6) has a composition of 3.29 Si p.f.u in good agreement with the compositions measured in the orthogneiss, mylonite and ultramylonite (3.25–3.30 Si p.f.u., Fig. 5) by Marquer (1987) and Challandes *et al.* (2008). The Tschermak substitution in white mica is strongly dependent on μCaO in the divariant stability field of the assemblage biotite–muscovite–epidote–albite–quartz while in Ca-free assemblages, the Si content in white mica is dependent only upon μMgO (Fig. 10c). Therefore, during the second stage of equilibration, when the rock evolves within the divariant field biotite–muscovite–epidote–albite–quartz towards the chlorite-bearing stability field, white mica is characterized by a continuous decrease in Si content from 3.29 to 3.14 p.f.u. at which point white mica is in equilibrium with the chlorite-bearing assemblage. This evolution of white mica composition is consistent with the composition of white mica measured in the chlorite-bearing ultramylonite, which ranges from 3.26 to 3.15 p.f.u. (Fig. 5). In the computed phase diagram, the XMg of biotite increases from 0.35 to 0.56 during K-feldspar breakdown, and then remains constant during epidote breakdown and chlorite crystallization, consistent with the observed biotite compositions (Fig. 10d).

DISCUSSION

Model of shear zone widening

Two different models of shear zone formation in granites are commonly invoked: dynamic localization and inherited-localization model (e.g. Mancktelow & Pennacchioni, 2005 for a review). In the former model (dynamic localization), the deformation induces local weakening and strain localization. The change in strength of the rock is due to mechanical and chemical processes such as grain size reduction, development of shape and crystallographic preferred orientation and metamorphic reactions. Gapais (1989) argued that the most favourable situation for strain localization and shear bands development in (meta-)granites is deformation during retrograde metamorphism. During cooling, the switch in deformation mechanism of feldspar from ductile to brittle deformation induces a local increase in strength of the rock and results in the development of shear bands to accommodate strain. Formation of classical shear bands in S–C–C′ structures can be attributed to this dynamic localization model (Berthé *et al.*, 1979). In contrast, the inherited-localization model implies a localization–propagation succession. It requires a brittle precursor along which the shear zone nucleates. According to Mancktelow & Pennacchioni (2005), mineral and chemical transformations produced during fluid infiltration induce a transition from brittle to ductile deformation and the formation of discrete shear zones that could eventually widen. A peculiarity of these shear zones is that they form an anastomosed network around weakly deformed or undeformed domains. Gapais (1989) suggested that discrete shear zones are likely to be formed in pretectonic granites during prograde and/or peak metamorphic conditions of deformation.

Preservation of large lenses of undeformed to weakly deformed granodiorite and the isobaric-isothermal conditions of the deformation support the inherited-model of shear zone formation in granitoids. The fundamental question addressed here is what drives the shear zone widening? There is no evidence of reaction- or strain-hardening that could increase the strength in the centre of the shear zone and induce the expansion of the shear zone into the surrounding weaker gneiss. In contrast, fluid-rock interactions and associated

© 2012 Blackwell Publishing Ltd

syn-kinematic reactions produce a large amount of well oriented phyllosilicates that form a weak interconnected network. Therefore, from a mechanical perspective, all strain should be accommodated by the weak high strain zone and the active deformation volume should remain constant or even decrease (Knipe & Wintsch, 1985).

An alternative model for shear zone widening would be to reduce the strength of the adjacent host-rock with increasing strain. This weakening is induced by the progressive equilibration of the metastable load-bearing assemblage of the host-rock at the *P–T–X–fluid* conditions of the deformation. In our conceptual model, the nucleation stage introduces a thermodynamic disequilibrium between the rocks in the precursor and the metastable magmatic assemblage of the host-rock. Chemical potential gradients cause diffuse alteration and weakening of the host rocks close to the shear zone. In this model, chemical processes, that are almost entirely driven by the metastability of the magmatic assemblage, may override mechanical processes in the formation of the shear zones. Preservation of magmatic assemblages at the *P–T* conditions of deformation is a very common scenario suggesting that the critical role of chemical processes in the evolution of shear zones is probably not restricted to the shear zone studied here. The chemical potential gradients produced between the metastable host-rock and the nucleated shear zone can also be referred as the isobaric isothermal reaction affinity that is defined by the difference in chemical potential of a component between the stable and metastable assemblage (e.g. Pattison *et al.*, 2011 and references therein).

Modelling metasomatism in granitic systems

Qualitative chemical potential (activity) diagrams have been used to understand fluid-rock equilibria in granitic systems under low grade metamorphic conditions (Wintsch, 1975; McCaig, 1984; Wintsch *et al.*, 1995). Although many studies have reported mass transfer of CaO, MgO with Na_2O and K_2O, phase diagrams were mostly constructed in Ca-free system with activity of K, Na and in a lesser extent Mg, as the main variables. Particular attention has been paid to ionic reactions of K-feldspar or albite breakdown into muscovite (e.g. Simpson & Wintsch, 1989; Wintsch *et al.*, 1995; Wibberley, 1999) like

$$3\mathrm{K-feldspar} + 2\mathrm{H}^+ = 1\mathrm{muscovite} + 6\mathrm{SiO_2} + 2\mathrm{K}^+$$

$$3\mathrm{Albite} + 2\mathrm{H}^+ + \mathrm{K}^+ = 1\mathrm{muscovite} + 6\mathrm{SiO_2} + 3\mathrm{Na}^+$$

The role of Ca-bearing phases, like plagioclase or epidote produced at the expense of magmatic plagioclase under greenschist to amphibolite facies conditions, has been underestimated (see Wintsch *et al.*, 2005 for an example in a calcium-bearing system). In this contribution, we show that the production of white mica and chlorite is induced by the breakdown of K-feldspar + albite + epidote (reactions 5, 6 & 7).

$$\mathrm{kf} + \mathrm{cz} + \mathrm{bio} + \mathrm{H_2O} + \mathrm{MgO} = \mathrm{mu} + \mathrm{q} + \mathrm{ab} + \mathrm{CaO} \quad (5)$$

$$\mathrm{kf} + \mathrm{ab} + \mathrm{bio} + \mathrm{H_2O} + \mathrm{MgO} = \mathrm{mu} + \mathrm{q} + \mathrm{cz} + \mathrm{Na_2O} \quad (6)$$

$$\mathrm{cz} + \mathrm{bio} + \mathrm{ab} + \mathrm{H_2O} + \mathrm{MgO} = \mathrm{chl} + \mathrm{mu} + \mathrm{q} + \mathrm{CaO} \quad (7)$$

This sequence of reactions is induced by the process of equilibration towards the composition of the chlorite-bearing ultramylonite. Quantitative chemical potential diagrams show that in a modelled granitic system with only MgO and CaO defined as mobile components, reactions (5) and (7) induce a relative loss of 100% of CaO coupled with an input of up to 139% of MgO. We suggest that the amount of mass transfer is controlled by the initial bulk composition to be equilibrated and the sequence of reactions and assemblages produced during the process of equilibration of the host-rock with the chlorite-bearing ultramylonite.

The good agreement between observed assemblages (mode and composition) with predicted assemblages by mineral equilibria modelling suggests that the equilibrium volume is at least larger than the volume of the sample used to measure the bulk rock composition (White *et al.*, 2008), that is, centimetre to decimetre cube. Although at the scale of the whole shear zone (metre-scale), disequilibrium probably still exists, we suggest that mineral thermodynamic equilibrium modelling is applicable to shear zone if local equilibrium is assumed. This result is not surprising because the fluid saturated conditions and deformation favours the transport of component and helps overpassing kinetic barriers to reach equilibrium.

Influence of mass transfer on syn-kinematic phase relations (phengite) and thermobarometric implications

Estimating *P–T–t* conditions of deformation, using shear zones is a major issue because phase relations are very sensitive to variations of fluid and bulk rock compositions during deformation. This effect has been highlighted looking at white mica because (i) it provides barometric informations, (ii) its fabric is used to decipher the deformation history and (iii) it can be in-situ dated with high spatial resolution by Ar-Ar laser extraction techniques (e.g. Challandes *et al.*, 2003; Di Vincenzo *et al.*, 2006).

Based on natural and experimental observations that the Si content per formula unit of phengite is dependent upon *P–T*, a geobarometer has been calibrated by Massone & Schreyer (1987). Although the application of this barometer has some important limitations, it has been extensively used over the past three decades. Therefore many *P–T* estimates, and

© 2012 Blackwell Publishing Ltd

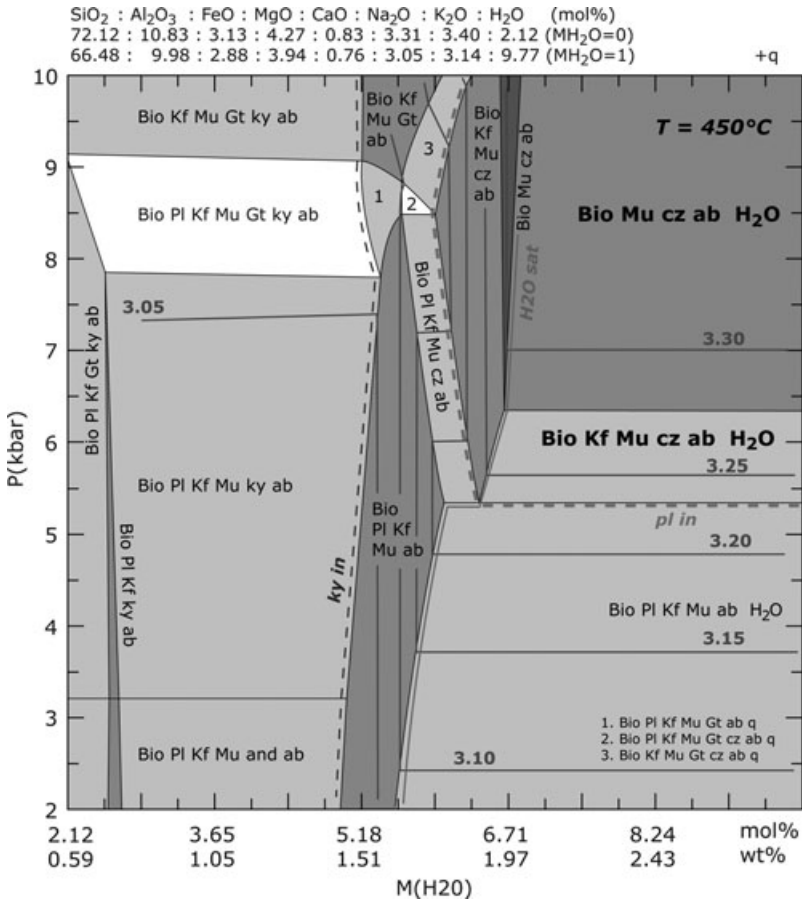

Fig. 11. P–MH_2O diagrams calculated at 450°C for the ultramylonite composition. The amount of water MH_2O varies from 2.12 to 9.76 mol%. Water saturation curve is shown as a red line and plagioclase-in and kyanite-in boundaries as dashed line. The Si-content per formula unit in phengite is contoured.

consequent geodynamic interpretations rely on this geobarometer. Application of the 'Si in phengite' barometer requires the coexistence of phengite with K-feldspar, phlogopite, quartz and H_2O in excess (Massone & Schreyer, 1987). If phengite is not in equilibrium with the limiting assemblage cited above (in most cases K-feldspar is missing) the barometer provides only a minimum pressure estimate (Massone & Schreyer, 1987). Although the slope and interval of the isopleths of Si p.f.u. in phengite contoured on the *P–T* sections of Fig. 5 are slightly different from those presented in fig. 5 of Massone & Schreyer (1987), their observation that Si content in phengite is dependent on the buffering assemblage is confirmed. More particularly, Fig. 5 shows that in the K-feldspar absent fields, the isopleths are shifted to significantly higher pressure. Such dependency of phengite composition and barometry upon mineral assemblages and the role of other components like CaO and Na_2O have also been pointed out by Wei *et al.* (2004) and Wei & Powell (2006).

Another assumption in the use of the phengite barometer is that water must be in excess. Massone & Schreyer (1987) have evaluated the effect of decreasing water activity and concluded that the effects on phengite composition are almost negligible although they have calculated a shift in pressure of ~3 kbar led by a decrease in water activity from 1.0 to 0.6. A P-M(H_2O) section calculated for the Grimsel ultramylonite composition, and contoured for the Si content of phengite, shows that a decrease in water content (below the water saturated conditions) at 6.5 kbar, would induce a rapid decrease in Si content of white mica from 3.28 to 3.05 (Fig. 11). This could be misinterpreted as decompression if the barometer of Massone & Schreyer (1987) is applied assuming that the system is fully saturated in water.

Similarly, mass transfer has a strong influence on phengite composition (Arancibia & Morata, 2005). The μMgO–μCaO section contoured for the Si content of white mica (Fig. 10c) shows that the process of equilibration of the host rock during the shear zone widening induces a decrease of Si-content of phengite from 3.29, when in equilibrium with K-feldspar + epidote + albite, to 3.14 p.f.u when white mica is in equilibrium with the chlorite-bearing assemblage at the same *P–T* conditions (Fig. 10c). In this case, the observation of low phengite-content mica in equilibrium with chlorite in the ultramylonite formed during syn-deformation metasomatism at peak metamorphic conditions might easily be misinterpreted as evidence for a low pressure retrograde

© 2012 Blackwell Publishing Ltd

deformation event corresponding to a decrease in pressure of ~4 kbar.

The preservation of a large and continuous range of phyllosilicate compositions is a common feature in rocks metamorphosed under 550°C (e.g. Trotet *et al.*, 2001; Vidal *et al.*, 2001, 2006 and references therein; De Andrade *et al.*, 2006). Vidal *et al.* (2006) suggested that if *P–T* conditions and oxidation state evolve during a deformation event, it is more favourable to maintain equilibrium by crystallizing new grains with a new composition rather than re-equilibrating the existing metastable grains by lattice diffusion. However, Vidal *et al.* (2006) also pointed out that the heterogeneity in phase chemistry might be due to local mass transfer along shear bands or schistosity planes, which act as preferential fluid pathways. We suggest that the role of micro- to macro-scale syn-deformation mass transfer and fluid conditions on white mica composition have been underestimated in the past and that some *P–T–t* evolutions might be revisited. For example, Duchêne *et al.* (2006) interpreted variations of phengite composition in shear zones in terms of decompression based on the application of the Massone & Schreyer (1987) barometer. This white mica has been dated to infer a rate of exhumation of 10 mm yr^{-1} (see fig. 9 in Duchêne *et al.*, 2006). Such *P–T–t* evolution and rate might be reconsidered if local mass transfer occurred during the syn-crystallization of the white mica.

To conclude the unique observation of variations of Si content in phengite across a strain gradient of a shear zone cannot simply be interpreted in terms of changes in *P–T* conditions during the deformation. It rather could reflect spatial variation of fluid conditions and amount of mass transfer.

ACKNOWLEDGEMENTS

This work is part of the PhD of E. Oliot and was supported by the French 'Ministère de l'Enseignement Supérieur et de la Recherche' and the University of Franche-Comté (BQR2006). We gratefully acknowledge V. de Andrade, O. Vidal (University of Grenoble, France) and P. Pitra (University of Rennes, France) for discussions on the modelling and white mica aspects, and N. Mancktelow and G. Pennacchioni for stimulating discussions on shear zone formation. M. Williams and T. Bell are acknowledged for the critical reviews and D. Aerden and D. Robinson for the careful editorial handling.

REFERENCES

Abrecht, J., 1994. Geologic units of the aar massif and their pre-alpine rock associations – a critical review. *Schweizerische Mineralogische und Petrographische Mitteilungen*, **74,** 5–27.

Arancibia, G. & Morata, D., 2005. Compositional variations of syntectonic white-mica in low-grade ignimbritic mylonite. *Journal of Metamorphic Geology*, **27,** 745–767.

Barnes, J.D., Selverstone, J. & Sharp, Z.D., 2004. Interactions between serpentinite devolatilization, metasomatism and strike-slip strain localization during deep-crustal shearing in the Eastern Alps. *Journal of Metamorphic Geology*, **22,** 283–300.

Baumgartner, L.P. & Olsen, S.N., 1995. A least-squares approach to mass-transport calculations using the isocon method. *Economic Geology and the Bulletin of the Society of Economic Geologists*, **90,** 1261–1270.

Berthé, D., Choukroune, P. & Jégouzo, P., 1979. Orthogneiss, mylonite and non coaxial deformation of granites: example of the south armorican shear zone. *Journal of Structural Geology*, **1,** 31–42.

Bialek, D., 1999. Chemical changes associated with deformation of granites under greenschist facies conditions: the example of the Zawidów Granodiorite (SE Lusatian Granodiorite Complex, Poland). *Tectonophysics*, **303,** 251–261.

Burlini, L. & Bruhn, D., 2005. High-strain zones: laboratory perspectives on strain softening during ductile deformation. In: *High-Strain Zones: Structure and Physical Properties* (eds Bruhn, D. & Burlini, L.), Vol. 245, pp. 1–24. Geological Society, Special Publications, London.

Challandes, N. 2001. Comportement des systèmes isotopiques ^{39}Ar–^{40}Ar et Rb-Sr dans les zones de cisaillement: exemples du massif de l'Aar (Massifs cristallins externes) et de la nappe de Suretta (Alpes centrales suisses). Thesis Univeristé de Neuchâtel, 271 pp

Challandes, N., Marquer, D. & Villa, I.M., 2003. Dating the evolution of C-S microstructures: a combined ^{39}Ar-^{40}Ar step-heating and UV laserprobe analysis of the Alpine Roffna shear zone. *Chemical Geology*, **197,** 3–19.

Challandes, N., Marquer, D. & Villa, I.M., 2008. *P-T-t* modelling, fluid circulation, and ^{39}Ar-^{40}Ar and Rb-Sr mica ages in the Aar Massif shear zones (Swiss Alps). *Swiss Journal of Geosciences*, **101,** 269–288.

Choukroune, P. & Gapais, D., 1983. Strain pattern in the Aar granite (central Alps) – orthogenesis developed by bulk inhomogeneous flattening. *Journal of Structural Geology*, **5,** 411–418.

Coggon, R. & Holland, T.J.B, 2002. Mixing properties of phengitic micas and revised garnet-phengite thermobarometers. *Journal of Metamorphic Geology*, **20,** 683–696.

Connolly, J.A.D., 1990. Multivariable phase diagrams: an algotithm based on generalized thermodynamics. *American Journal of Science*, **290,** 666–718.

Connolly, J.A.D., 2005. Computation of phase equilibria by linear programming: a tool for geodynamic modelling and its application to subduction zone decarbonation. *Earth and Planetary Science Letters*, **236,** 524–541.

De Andrade, V., Vidal, O., Lewin, E., O'Brien, P. & Agard, P., 2006. Quantification of electron microprobe compositional maps of rock thin sections: an optimized method and examples. *Journal of Metamorphic Geology*, **24,** 655–668.

Demény, A., Sharp, Z.D. & Pfeiffer, H.R., 1997. Mg-metasomatism and formation conditions of Mg-chlorite-muscovite-quartzphyllites (leucophyllites) of the Eastern Alps (W Hungary) and their relations to Alpine whiteschists. *Contribution to Mineralogy and Petrology*, **128,** 247–260.

Di Vincenzo, G., Tonarini, S., Lombardo, B., Castelli, D. & Ottolini, L., 2006. Comparison of ^{39}Ar-^{40}Ar and Rb-Sr data on phengites from the UHP Brossasco-Isasca unit (Dora Maira Massif, Italy): implications for dating white mica. *Journal of Petrology*, **47,** 1439–1465.

Dipple, G.M. & Ferry, J.M., 1992. metasomatism and fluid-flow in ductile fault zones. *Contributions to Mineralogy and Petrology*, **112,** 149–164.

Duchêne, S., Aissa, R. & Vanderhaeghe, O., 2006. Pressure-temperature-time evolution of metamorphic rocks from naxos (Cyclades, Greece): constraints from thermobarometry and Rb/Sr dating. *Geodinamica Acta*, **19,** 301–321.

Fitz Gerald, J. & Stünitz, H., 1993. Deformation of granitoids at low metamorphic grade. I: reactions and grain size reduction. *Tectonophysics*, **221,** 269–297.

© 2012 Blackwell Publishing Ltd

Fourcade, S., Marquer, D. & Javoy, M., 1989. $^{18}O/^{16}O$ variations and fluid circulation in a deep shear zone – the case of the alpine ultramylonites from the aar massif central Alps, Switzerland. *Chemical Geology*, **77,** 119–131.

Gapais, D., 1989. Shear structures within deformed granites – mechanical and thermal indicators. *Geology*, **17,** 1144–1147.

Gapais, D., Bale, P., Choukroune, P., Cobbold, P.R., Mahjoub, Y. & Marquer, D., 1987. Bulk kinematics from shear zone patterns – some field examples. *Journal of Structural Geology*, **9,** 635–646.

Glodny, J. & Grauert, B., 2009. Evolution of a hydrothermal fluid-rock interaction system as recorded by Sr isotopes: a case study from the Schwarzwald, SW Germany. *Mineralogy and Petrology*, **95,** 163–178.

Groome, W., Johnson, S. & Koons, P., 2006. The effects of porphyroblast growth on the effective viscosity of metapelitic rocks: implications for the strength of the middle crust. *Journal of Metamorphic Geology*, **24,** 389–407.

Guermani, A. & Pennacchioni, G., 1998. Brittle precursors of plastic deformation in a granite: an example from the Mont Blanc massif (Helvetic, western Alps). *Journal of Structural Geology*, **20,** 135–148.

Gueydan, F., Leroy, Y.M., Jolivet, L. & Agard, P., 2003. Analysis of continental midcrustal strain localization induced by microfracturing and reaction-softening. *Journal of Geophysical Research – Solid Earth*, **108**(B2)**,** 2064.

Hippert, J.F., 1998. Breakdown of feldspar, volume gain and lateral mass transfer during mylonitization of granitoid in a low metamorphic grade shear zone. *Journal of Structural Geology*, **20,** 175–193.

Holland, T.J.B. & Powell, R., 1998. An internally consistent thermodynamic data set for phases of petrological interest. *Journal of Metamorphic Geology*, **16,** 309–343.

Holyoke, C.W. & Tullis, J., 2006. The interaction between reaction and deformation: an experimental study using a biotite plus plagioclase plus quartz gneiss. *Journal of Metamorphic Geology*, **24,** 743–762.

Ingles, J., Lamouroux, C., Soula, J., Guerrero, N. & Debat, P., 1999. Nucleation of ductile shear zones in a granodiorite under greenschist facies conditions, Neouvielle massif, Pyrenees, France. *Journal of Structural Geology*, **21,** 555–576.

Johnson, S.E., Jin, Z., Naus-Thijssen, F.M.J. & Koons, P.O., 2011. Coupled deformation and metamorphism in the roof of a tabular midcrustal igneous complex. *Geological Society of America Bulletin*, **123,** 1016–1032.

Keller, L.M., Abart, R., Stünitz, H. & Capitani, C.D., 2004. Deformation, mass transfer and mineral reactions in an eclogite facies shear zone in a polymetamorphic metapelite (Monte Rosa nappe, western Alps). *Journal of Metamorphic Geology*, **22,** 97–118.

Knipe, R.J. & Wintsch, R.P., 1985. Heterogeneous deformation, foliation development, and metamorphic processes in a polyphase mylonite. In: *Metamorphic reactions. kinetics, textures and deformation* (eds Thompson, A.B. & Rubie, D.C.), pp. 180–210. Springer-Verlag, New York.

Korzhinskii, D.S., 1970. *Theory of metasomatic zoning*. Oxford University press, Oxford, 162 pp.

Labhart, T.P., 1977. *Aarmassiv und Gotthardmassiv. Sammlung geologischer Fuehrer*. Gebrüder Borntraeger, Berlin, Stuttgart, 173 pp.

Mancktelow, N. & Pennacchioni, G., 2005. The control of precursor brittle fracture and fluid-rock interaction on the development of single and paired ductile shear zones. *Journal of Structural Geology*, **27,** 645–661.

Marquer, D., 1987. Transfert de matière et déformation progressive des granitoïdes. Exemples des massifs de l'Aar et du Gotthard (Alpes central suisses), Thesis Université de Rennes, 250 pp.

Marquer, D., 1989. Transfert de matière et déformation des granitoïdes. Aspects méthodologiques. *Schweizer Mineralogische und Petrographische Mitteilungen*, **69,** 15–35.

Marquer, D. & Burkhard, M., 1992. Fluid circulation, progressive deformation and mass-transfer processes in the upper crust – the example of basement cover relationships in the external crystalline massifs, Switzerland. *Journal of Structural Geology*, **14,** 1047–1057.

Marquer, D., Gapais, D. & Capdevila, R., 1985. chemical-changes and mylonitization of a granodiorite within low-grade metamorphism (Aar massif, central Alps). *Bulletin de Minéralogie*, **108,** 209–221.

Massone, H.J. & Schreyer, W., 1987. Phengite geobarometry based on the limiting assemblage with k-feldspar, phlogopite, and quartz. *Contributions to Mineralogy and Petrology*, **96,** 212–224.

McCaig, A.M., 1984. Fluid-rock interaction in some shear zones from the pyrenees. *Journal of Metamorphic Geology*, **2,** 129–141.

Means, W.D., 1995. Shear zones and rock history. *Tectonophysics*, **247,** 157–160.

Mitra, G., 1978. Ductile deformation zones and mylonites – mechanical processes involved in deformation of crystalline basement rocks. *American Journal of Science*, **278,** 1057–1084.

Montési, L. & Zuber, M., 2002. A unified description of localization for application to large-scale tectonics. *Journal of Geophysical Research – Solid Earth*, **107**(B3)**,** 2045.

Newton, R.C. & Haselton, E.C., 1981. Thermodynamics of the garnet-plagioclase-Al_2SiO_5-quartz geobarometer. In: *Thermodynamics of Minerals and Melts. Advances in Physical Geochemistry* (eds Newton, R.C., Navrotsky, A. & Wood, B. J.), pp. 129–145. Springer-Verlag, New-York.

Oliot, E., Goncalves, P. & Marquer, D., 2010. Role of plagioclase and reaction softening in a metagranite shear zone at mid-crustal conditions (Gotthard Massif, Swiss Central Alps). *Journal of Metamorphic Geology*, **28,** 849–871.

Pattison, D.R.M., De Capitani, C. & Gaidies, F., 2011. Petrological consequences of variations in metamorphic reaction affinity. *Journal of Metamorphic Geology*, **29,** 953–978.

Pennacchioni, G., 2005. Control of the geometry of precursor brittle structures on the type of ductile shear zone in the Adamello tonalites, Southern Alps (Italy). *Journal of Structural Geology*, **27,** 627–644.

Pennacchioni, G. & Mancktelow, N.S., 2007. Nucleation and initial growth of a shear zone network within compositionally and structurally heterogeneous granitoids under amphibolite facies conditions. *Journal of Structural Geology*, **29,** 1757–1780.

Poirier, J., 1980. Shear localization and shear instability in materials in the ductile field. *Journal of Structural Geology*, **2,** 135.

Rossi, M., Rolland, Y., Vidal, O. & Cox, S.F., 2005. Geochemical variations and element transfer during shear zone development and related episyenites at middle crust depths: insights from the Mont-Blanc granite (French-Italian Alps). In: *High Strain Zones: Structure and Physical Properties* (eds Bruhn, D. & Burlini, L.), pp. 373–396. Geological Society of London, Special Publications, London.

Rutter, E.H., 1999. On the relationship between the formation of shear zones and the form of the flow law for rocks undergoing dynamic recrystallization. *Tectonophysics*, **303,** 147–158.

Sassier, C., Boulvais, P., Gapais, D., Capdevila, R. & Diot, H., 2006. From granitoid to kyanite-bearing micaschist during fluid-assisted shearing (Ile d'Yeu, France). *International Journal of Earth Science*, **95,** 2–18.

Schaltegger, U., 1994. Unraveling the premesozoic history of Aar and Gotthard massifs (Central Alps) by isotopic dating – a review. *Schweizerische Mineralogische und Petrographische Mitteilungen*, **74,** 41–51.

Segall, P. & Simpson, C., 1986. Nucleation of ductile shear zones on dilatant fractures. *Geology*, **14,** 56–59.

Selverstone, J., Morteani, G. & Staude, J., 1991. Fluid channelling during ductile shearing: transformation of granodiorite

© 2012 Blackwell Publishing Ltd

into aluminous schist in the Tauern Window, Eastern Alps. *Journal of Metamorphic Geology*, **9,** 419–431.

Simpson, C., 1985. Deformation of granitic-rocks across the brittle ductile transition. *Journal of Structural Geology*, **7,** 503–511.

Simpson, C. & Wintsch, R.P., 1989. Evidence for deformation-induced K-feldspar replacement by myrmekite. *Journal of Metamorphic Geology*, **7,** 261–275.

Steck, A., 1968. Die alpinischen strkturen in den zentralen Aargraniten des westlichen Aarmassivs: the Alpine structures in the central Aar granite of the western part of theAar massif. *Eclogae Geologicae Helvetica*, **61,** 19–48.

Steck, A., 1984. Tertiary deformation structures in the Central Alps. *Eclogae Geologicae Helvetiae*, **77,** 55–\&.

Stunitz, H. & Tullis, J., 2001. Weakening and strain localization produced by syn-deformational reaction of plagioclase. *International Journal of Earth Sciences*, **90,** 136–148.

Trotet, F., Vidal, O. & Jolivet, L., 2001. Exhumation of Syros and Sifnos metamorphic rocks (Cyclades, Greece). New constraints on the P-T paths. *European Journal of Mineralogy*, **13,** 901–920.

Tullis, J., Yund, R. & Farver, J., 1996. Deformation-enhanced fluid distribution in feldspar aggregates and implications for ductile shear zones. *Geology*, **24,** 63–66.

Vidal, O., Parra, T. & Trotet, F., 2001. A thermodynamic model for Fe-Mg aluminous chlorite using data from phase equilibrium experiments and natural pelitic assemblages in the 100 degrees to 600 degrees C, 1 to 25 kb range. *American Journal of Science*, **301,** 557–592.

Vidal, O., De Andrade, V., Lewin, E., Munoz, M., Parra, T. & Pascarelli, S., 2006. *P-T*-deformation-Fe^{3+}/Fe^{2+} mapping at the thin section scale and comparison with XANES mapping: application to a garnet-bearing metapelite from the Sambagawa metamorphic belt (Japan). *Journal of Metamorphic Geology*, **24,** 669–683.

Vitale, S. & Mazzoli, S., 2008. Heterogeneous shear zone evolution: the role of shear strain hardening/softening. *Journal of Structural Geology*, **30,** 1383–1395.

Waldbaum, D.R. & Thompson, J.B., 1969. Mixing properties of sanidine crystalline solutions: IV. Phase diagrams from equations of state. *American Mineralogist*, **54,** 1274–1298.

Wei, C.J. & Powell, R., 2006. Calculated phase relations in the system NCKFMASH (Na_2O-CaO-K_2O-FeO-MgO-Al_2O_3-SiO_2-H_2O) for high-pressure metapelites. *Journal of Petrology*, **47,** 385–408.

Wei, C.J., Powell, R. & Clarke, G.L., 2004. Calculated phase equilibria for low- and medium-pressure metapelites in the KFMASH and KMnFMASH systems. *Journal of Metamorphic Geology*, **22,** 495–508.

White, S. & Knipe, R., 1978. Microstructure and cleavage development in selected slates. *Contributions to Mineralogy and Petrology*, **66,** 165–174.

White, R.W., Powell, R. & Holland, T.J.B., 2007. Progress relating to calculation of partial melting equilibria for metapelites. *Journal of Metamorphic Geology*, **25,** 511–527.

White, R.W., Powell, R. & Baldwin, J.A., 2008. Calculated phase equilibria involving chemical potentials to investigate the textural evolution of metamorphic rocks. *Journal of Metamorphic Geology*, **26,** 181–198.

Wibberley, C., 1999. Are feldspar-to-mica reactions necessarily reaction-softening processes in fault zones? *Journal of Structural Geology*, **21,** 1219–1227.

Wintsch, R.P., 1975. Solid-fluid equilibria in system $KAlSi_3O_8$-$NaAlSi_3O_8$-Al_2SiO_5-SiO_2-H_2O-HCl. *Journal of Petrology*, **16,** 57–79.

Wintsch, R.P., Christoffersen, R. & Kronenberg, A.K., 1995. Fluid-rock reaction weakening of fault zones. *Journal of Geophysical Research – Solid Earth*, **100,** 13021–13032.

Wintsch, R., Aleinikoff, J. & Keewook, Y., 2005. Foliation development and reaction softening by dissolution and precipitation in the transformation of granodiorite to orthogneiss, Glastonbury Complex, Connecticut, USA. *Canadian Mineralogist*, **43,** 327–347.

Yonkee, W.A., Parry, W.T. & Bruhn, R.L., 2003. Relations between progressive deformation and fluid-rock interaction during shear-zone growth in a basement-cored thrust sheet, Sevier orogenic belt, Utah. *American Journal of Science*, **303,** 1–59.

Received 20 December 2011; revision accepted 15 May 2012.

© 2012 Blackwell Publishing Ltd